NASA CONTRACTOR REPORT

NASA CR-2698

NASA CR-26

FINITE ELEMENT COMPUTER PROGRAM
TO ANALYZE CRACKED ORTHOTROPIC SHEETS

C. S. Chu, J. M. Anderson,
W. J. Batdorf, and J. A. Aberson

NATIONAL AERONAUTICS AND SPACE ADMINISTRATION • WASHINGTON, D. C. • JULY 1976

1. Report No. NASA CR-2698	2. Government Accession No.	3. Recipient's Catalog No.
4. Title and Subtitle FINITE ELEMENT COMPUTER PROGRAM TO ANALYZE CRACKED ORTHOTROPIC SHEETS		5. Report Date JULY 1976
		6. Performing Organization Code
7. Author(s) C. S. Chu; J. M. Anderson; W. J. Batdorf; and J. A. Aberson		8. Performing Organization Report No.
		10. Work Unit No.
9. Performing Organization Name and Address Lockheed Aircraft Corporation Lockheed-Georgia Company 86 South Cobb Drive Marietta, GA 30060		11. Contract or Grant No. NAS1-13605
		13. Type of Report and Period Covered Contractor Report
12. Sponsoring Agency Name and Address National Aeronautics and Space Administration Washington D.C. 20546		14. Sponsoring Agency Code 743-01-11-02

15. Supplementary Notes
FINAL REPORT Langley Technical Monitor: C. C. Poe, Jr.

16. Abstract

A finite-element computer program was developed to analyze a two-dimensional orthotropic sheet with through-the-thickness cracks and temperature gradient. The program includes special crack-tip elements that account for the singular stress fields associated with crack opening (Mode I) and crack sliding (Mode II) displacements at the crack tip. The program also includes a linear spring element and a constant-strain, triangular element. A number of problems for which closed-form solutions exist were analyzed to demonstrate the capabilities of the program.

17. Key Words (Suggested by Author(s)) orthotropic; composite materials; finite element; crack; crack-tip element; stress intensity factor; thermal; computer program	18. Distribution Statement Unclassified-Unlimited Subject Category 39	
19. Security Classif. (of this report) Unclassified	20. Security Classif. (of this page) Unclassified	21. No. of Pages 87
		22. Price* $4.75

TABLE OF CONTENTS

TABLE OF CONTENTS (Continued)

LIST OF FIGURES

LIST OF FIGURES - Continued

LIST OF TABLES

FINITE ELEMENT COMPUTER PROGRAM TO ANALYZE CRACKED ORTHOTROPIC SHEETS

By

Chorng-Shin Chu
J. M. Anderson*
W. J. Batdorf
J. A. Aberson**

SUMMARY

The objective of this study was to develop a finite-element computer program that performs a two-dimensional elastostatic analysis of plane anisotropic homogeneous sheets with a through-the-thickness crack. The program includes special crack-tip elements that account for the singular stress fields associated with crack opening (Mode I) and sliding (Mode II) displacements at the crack tips. These special crack-tip elements provide a new tool for computing stress-intensity factors, and they can be used for predicting the crack propagation for a damaged structure.

Two types of crack elements have been developed. One element has 8 nodes and is restricted to symmetric applications; the other element has 10 nodes and is capable of representing the crack-tip neighborhood when both the crack opening and sliding modes of deformation occur. The 8-node symmetric cracked element takes full advantage of the symmetry, so that only one-half of a configuration which is symmetric about a line containing the crack need be modeled. However, the 10-node unsymmetric cracked element has much wider usage in practical fracture-mechanics applications.

These cracked elements can exhibit either anisotropic or isotropic behavior. (Orthotropic materials are considered a special case of anisotropic material.) A stress function in a half-power series form appropriate to the crack tip neighborhood is chosen to formulate the stiffness matrix for the anisotropic cracked elements, and a Williams' series stress function is used for the isotropic cracked elements.

*Consultant, Associate Professor, School of Engineering Science and Mechanics, Georgia Institute of Technology.

**Consultant, Assistant Professor, School of Engineering Science and Mechanics, Georgia Institute of Technology.

The computer program contains an axial element, a linear spring element, a triangular element, and isotropic and anisotropic cracked elements. Thermal-strain analysis capability is included. Extensive tests during the development stage have been made in order to validate the program against known solutions. To illustrate the capabilities of these two types of cracked elements, a number of selected sample problems are presented in this report for demonstrations. The computer program has proved to be very efficient.

INTRODUCTION

The finite-element method is one of the most effective approaches available for plane elasticity problems having irregular boundaries or discontinuous boundary conditions. Early efforts to bring this method to bear on crack problems depended on the use of many conventional elements around the crack tip in an attempt to represent the extreme stress gradients there. Stress-intensity factors were estimated from results obtained with such models either by extrapolating crack-opening displacement (ref. 1) or by numerically computing the variation in strain energy with crack length (ref. 2). Such conventional methods have been found to be limited and uneconomical. For example, Oglesby and Lomacky (ref. 3) have indicated that the maximum permissible element size necessary to ensure acceptable accuracy (5% error or less) is on the order of 1/500 of the crack half length.

To circumvent this economic problem, development and research efforts have turned toward formulating elements which contain the crack-tip stress singularity. These special singularity elements, usually referred to as cracked finite elements, represent a significant improvement in both accuracy and economy in comparison with conventional methods. Many cracked finite elements developed to date (ref. 4-8) incorporate only the singular term in the series expansion for the crack-tip stress field. Admittedly, this term dominates all others near the crack tip, but to guarantee that the nonsingular contributions are comparably negligible, the neighborhood represented by the cracked element must be quite small, and the problem of economy arises again. Moreover, the neighboring conventional elements in such instances are drawn very near the crack tip again, and concern over their capability to represent the stress field adequately has led some investigators to introduce special "border elements" having a higher degree of sophistication than that routinely required for plane elasticity problems.

Wilson (ref. 9) has developed a cracked finite element that makes use of the first four terms in the expansion for the crack-tip stress field. He reports accurate results when this element is used in conjunction with a fairly modest number of conventional elements. Wilson's element, however, has the disadvantage of being semi-circular and hence is somewhat awkward to use with conventional elements, which almost always have straight boundaries. Moreover, Wilson's element (as well as some others previously referenced) has fewer degrees of freedom than are needed for independence of the nodal displacements. This requires that the stiffness matrix of the cracked element receive special attention in forming the stiffness matrix of the assembly.

2

Early in 1973, the Lockheed-Georgia Company completed the development of isotropic versions of two high-order cracked finite elements, i.e., elements that incorporate many terms in the expansion for the crack-tip stress field. This feature permits very accurate esti-mates of stress-intensity factors with relatively coarse finite-element grids. Both high-order cracked elements, one for symmetric (Mode I) applications and one for unsymmetric (Mode I and Mode II) applications, have a perfect balance between actual degrees of freedom and the number of nodal displacement components. Thus, the numerical analyst adds the cracked element to an assembly in exactly the same way that he adds a conventional element. The shape of each element was chosen to make it fit conveniently in models making use of the most widely used membrane element: the constant-strain triangle. The remarkable accuracy obtained with both elements in isotropic applications using very coarse finite-element repre-sentations (ref. 10) would seem to indicate that the periodic concern of some investigators over the displacement incompatibility that exists at the interface of the high-order cracked element and a conventional element is largely academic.

The continually increasing use of fiber-reinforced composites in aerospace applications, coupled with a growing confidence in the ability of linear elastic fracture mechanics (LEFM) to predict the growth rate and stability of cracks in isotropic materials, has lately resulted in considerable interest in the prospects of successfully applying LEFM to anisotropic materials (ref. 11). This report contains the analytical background and an account of several numeri-cal modifications and additions required to effect the following principal extensions of Lockheed-Georgia's existing analysis capability for cracked isotropic structures:

- o Axial element

- o Anisotropic constant-strain triangle

- o Anisotropic cracked elements

- o Automatic node sequencing to minimize bandwidth

- o Input-data generator

- o Thermal stress analysis capability

SYMBOLS

$\{P\}$ Vector of forces for uncoupled structure

$\{P\}$ Vector of displacements for uncoupled structure

$\{P_{rt}\}$ Vector of thermal forces for complete restraint of uncoupled structure

$[k]$ Uncoupled stiffness matrix

$\{q\}$ Vector of displacements for coupled structure

$\{Q\}$	Vector for forces for coupled structure
$[\psi]$	Compatibility matrix for displacements
$[K]$	Coupled stiffness matrix
$\{Q_{rt}\}$	Vector of thermal forces for complete restraint of coupled structure
$\{\sigma\}$	Stress vector
$\{\epsilon\}$	Strain vector
$[A_e]$	Elastic matrix for Hooke's law in local axis
$[A_m]$	Elastic matrix for Hookes law in material axis
$[U]$	Transformation matrix for elastic coefficients
$\{\alpha\}$	Vector representing thermal expansion coefficients
x, y, z	Rectangular coordinates
r, θ	Polar coordinates
$\sigma_x, \sigma_y, \sigma_z$	Normal components of stress parallel to x-, y-, and z-axes
$\tau_{xy}, \tau_{xz}, \tau_{yz}$	Shearing-stress components in rectangular coordinates
$\epsilon_x, \epsilon_y, \epsilon_z$	Unit elongations in x-, y-, and z-directions
$\gamma_{xy}, \gamma_{xz}, \gamma_{yz}$	Shearing-strain components in rectangular coordinates
σ_r, σ_θ	Radial and tangential normal stresses in polar coordinates
$\tau_{r\theta}$	Shearing stress in polar coordinates
$\epsilon_r, \epsilon_\theta$	Radial and tangential unit elongation in polar coordinates
E	Modulus of elasticity in tension and compression
G	Modulus of elasticity in shear
ν	Poisson's ratio
V	Strain energy
T	Temperature

4

U	Stress function
a	Half crack length
L	Total height of cracked tension plate
W	Total width of cracked tension plate
w	$= W/2$
a/w	Crack length aspect ratio

BASIC EQUATIONS FOR FINITE ELEMENT PROGRAM

Matrix Equations for Stiffness Method

The finite element analysis program is based on the direct stiffness method. With this approach, a complex structure is idealized as an assembly of simple elements; for example: axial elements, triangular membrane elements (isotropic and anisotropic), and 8- and 10-node cracked elements. Each of these elements, separately, can be analyzed without difficulty. By expressing the various mathematical relationships in matrix form, it is possible to assemble automatically a large number of discrete elements to simulate almost any complex structure. The basic matrix operations that are executed by the program are illustrated here. These equations include thermal effects.

In matrix form, the uncoupled force-displacement equation for a single element or the entire structure can be written as

$$\{P\} = [k]\{p\} + \{P_{rt}\} \tag{1}$$

where P and p are vectors of forces and displacements, respectively, and k is the uncoupled stiffness matrix. The term P_{rt} is a vector of thermal forces equivalent to the forces produced when each element is completely restrained.

From compatibility considerations we can define ψ such that

$$\{p\} = [\psi]\{q\} = [\psi_a \quad \psi_b]\begin{Bmatrix} q_a \\ q_b \end{Bmatrix} \tag{2}$$

where q is a vector of node point displacements for the coupled structure. In other words the p vector is referred to the local uncoupled system and q to the coupled structure defined in some global reference frame. The matrix ψ consists of direction cosines and is determined by the topology of the structural model. The vector q can then be expressed in terms of unknown displacements q_a and known displacements q_b. From the principal of virtual work it can be shown that

$$\{Q\} = [\psi^T k \psi]\{q\} + [\psi^T]\{P_{rt}\} \tag{3}$$

or

$$\{Q\} = [K]\{q\} + \{Q_{rt}\} \tag{4}$$

Equation (4) is then the force-displacement equation for the coupled or global system, where Q and q are forces and displacements, respectively. The vector Q_{rt} represents forces for complete restraint for the global system. Equation (4) can be expanded as

$$\left\{ \begin{matrix} Q_a \\ Q_b \end{matrix} \right\} = \begin{bmatrix} K_{aa} & K_{ab} \\ K_{ba} & K_{bb} \end{bmatrix} \left\{ \begin{matrix} q_a \\ q_b \end{matrix} \right\} + \left\{ \begin{matrix} Q_{art} \\ Q_{brt} \end{matrix} \right\} \tag{5}$$

where Q_a and q_a are applied forces and unknown displacements; and Q_b and q_b are reaction forces and known displacements. To determine the elastic displacements for a hot structure it is then necessary to solve the following set of linear equations:

$$\left\{ Q_a - K_{ab} q_b - Q_{art} \right\} = \begin{bmatrix} K_{aa} \end{bmatrix} \left\{ q_a \right\} \tag{6}$$

Once the displacements are known, the loads in each discrete element can then be determined from the following equation

$$\left\{ P \right\} = \begin{bmatrix} k \end{bmatrix} \begin{bmatrix} \psi \end{bmatrix} \left\{ q \right\} + \left\{ P_{rt} \right\} \tag{7}$$

The reaction forces, along with the equilibrium check, can be determined from Equation (8)

$$\left\{ Q \right\} = \begin{bmatrix} \psi^T \end{bmatrix} \left\{ P \right\} \tag{8}$$

References (12) and (13) discuss the various concepts of matrix analysis of structures. The derivations of the element stiffness matrices, except for the cracked elements, are outlined in the Appendix.

Transformation of Elastic and Thermal Coefficients

For a two-dimensional elastic plate the relationship between stress and strain can be written as

$$\left\{ \sigma \right\} = \begin{bmatrix} A_e \end{bmatrix} \left\{ \epsilon \right\} \tag{9}$$

For an isotropic material and plane-stress conditions,

$$\begin{bmatrix} A_e \end{bmatrix} = \begin{bmatrix} \dfrac{E}{1-\nu^2} & \dfrac{\nu E}{1-\nu^2} & 0 \\[3mm] \dfrac{\nu E}{1-\nu^2} & \dfrac{E}{1-\nu^2} & 0 \\[3mm] 0 & 0 & G \end{bmatrix} \tag{10}$$

In the general case of anisotropic materials the only requirement is that the matrix of coefficients be symmetric, that is

$$[A_e] = \begin{bmatrix} A_{11} & A_{12} & A_{16} \\ A_{12} & A_{22} & A_{26} \\ A_{16} & A_{26} & A_{66} \end{bmatrix} \qquad (11)$$

The six coefficients are defined with respect to a material axis whose orientation usually does not correspond to the principal axis of the structural element. The transformation matrix used within the program to rotate the elastic coefficients was expressed in terms of direction cosines. It is very important to note that all the angles are measured from the local axis to the material axis (see figure 1).

The transformation for the elastic coefficients is then

$$[A_e]_{local} = [U]^T [A_m]_{mat'l} [U] \qquad (12)$$

where

$$[U] = \begin{bmatrix} \cos^2\alpha & \cos^2\beta & \cos\alpha \ \cos\beta \\ \cos^2\beta & \cos^2\alpha & -\cos\alpha \ \cos\beta \\ -2\cos\alpha \ \cos\beta & 2\cos\alpha \ \cos\beta & \cos^2\alpha - \cos^2\beta \end{bmatrix}$$

and for the thermal expansion coefficient vector

$$\begin{Bmatrix} \alpha_{11} \\ \alpha_{22} \\ \alpha_{12} \end{Bmatrix}_{local} = [U]^{-1} \begin{Bmatrix} \alpha_{11} \\ \alpha_{22} \\ \alpha_{12} \end{Bmatrix}_{mat'l} \qquad (13)$$

In the computer program all these transformations are performed automatically for each element. It is only necessary to indicate the direction of the material axis by specifying two points on the axis. Several material axes can be specified for a single structural model.

TWO-DIMENSIONAL ELASTIC SOLUTIONS FOR
CRACK-TIP STRESSES AND DISPLACEMENTS

The field equations of elasto statics appropriate to isothermal deformation under plane-stress conditions ($\sigma_z = \tau_{yz} = \tau_{zx} = 0$) with zero body forces are given below and represent a basis for all the equations developed in this section.

$$\epsilon_x = \frac{\partial u_x}{\partial x} \ , \quad \epsilon_y = \frac{\partial u_y}{\partial y} \quad \text{and} \quad \gamma_{xy} = \frac{\partial u_x}{\partial y} + \frac{\partial u_y}{\partial x} \tag{14}$$

$$\frac{\partial^2 \epsilon_x}{\partial y^2} + \frac{\partial^2 \epsilon_y}{\partial x^2} = \frac{\partial^2 \gamma_{xy}}{\partial x \partial y} \tag{15}$$

$$\begin{Bmatrix} \epsilon_x \\ \epsilon_y \\ \gamma_{xy} \end{Bmatrix} = \begin{bmatrix} a_{11} & a_{12} & a_{16} \\ a_{12} & a_{22} & a_{26} \\ a_{16} & a_{26} & a_{66} \end{bmatrix} \begin{Bmatrix} \sigma_x \\ \sigma_y \\ \tau_{xy} \end{Bmatrix} \tag{16}$$

$$\frac{\partial \sigma_x}{\partial x} + \frac{\partial \tau_{xy}}{\partial y} = 0 \tag{17}$$

and

$$\frac{\partial \sigma_y}{\partial y} + \frac{\partial \tau_{xy}}{\partial x} = 0$$

For plane-strain applications ($\epsilon_z = \gamma_{yz} = \gamma_{zx} = 0$), the constants a_{ij} in (16) must be replaced by their plane-strain counterparts β_{ij} given by

$$\beta_{ij} = a_{ij} - \frac{a_{i3} a_{j3}}{a_{33}} \quad (i, j = 1, 2, 6) \tag{18}$$

The form of the equilibrium equations (17) implies the existence of a stress function $U(x, y)$ such that

$$\sigma_x = \frac{\partial^2 U}{\partial y^2} \ , \quad \sigma_y = \frac{\partial^2 U}{\partial x^2} \quad \text{and} \quad \tau_{xy} = -\frac{\partial^2 U}{\partial x \partial y} \tag{19}$$

9

By using (19) to eliminate the stress components in (16) and substituting the resulting strain components into the compatibility condition (15), we find that the stress function must satisfy

$$a_{22} \frac{\partial^4 U}{\partial x^4} - 2a_{26} \frac{\partial^4 U}{\partial x^3 \partial y} + (2a_{12} + a_{66}) \frac{\partial^4 U}{\partial x^2 \partial y^2} - 2a_{16} \frac{\partial^4 U}{\partial x \partial y^3} + a_{11} \frac{\partial^4 U}{\partial y^4} = 0 \tag{20}$$

Equation (20) may be written as the product of four first-order operators

$$D_i = \frac{\partial}{\partial y} - \mu_i \frac{\partial}{\partial x} \quad (i = 1, \ldots 4) \tag{21}$$

If μ_1, μ_2, μ_3 and μ_4 are roots of the characteristic polynomial,

$$a_{11} \mu^4 - 2a_{16} \mu^3 + (2a_{12} + a_{66}) \mu^2 - 2a_{26} \mu + a_{22} = 0 \tag{22}$$

then (20) may be written as

$$D_1 D_2 D_3 D_4 \, U(x, y) = 0 \tag{23}$$

The roots of (22) occur in complex-conjugate pairs and can be shown by energy considerations always to have non-zero imaginary parts. The designation μ_1, μ_2, $\bar{\mu}_1$ and $\bar{\mu}_2$ shall henceforth be used for the roots of (22), and it will be taken for granted that $\mu_i - \bar{\mu}_i \neq 0$. The general solution of (23) for $U(x, y)$ can now be written by repeated integration, but the form it takes depends on whether or not the roots of (22) are distinct. A discussion of cases follows.

<div align="center">Distinct Roots ($\mu_1 \neq \mu_2$)</div>

For distinct roots, the general solution of (23) for real $U(x, y)$ is

$$U(x, y) = 2 \mathrm{Re}[U_1(z_1) + U_2(z_2)] \tag{24}$$

where U_1 and U_2 are arbitrary functions of the complex variables

$$z_1 = x + \mu_1 y \quad \text{and} \quad z_2 = x + \mu_2 y \tag{25}$$

respectively. Upon substituting (24) into (19) the following expressions are found for the stress components.

$$\sigma_x = 2 \mathrm{Re}[\mu_1^2 U_1''(z_1) + \mu_2^2 U_2''(z_2)]$$

$$\sigma_y = 2 \mathrm{Re}[U_1''(z_1) + U_2''(z_2)] \tag{26}$$

10

and $\quad \tau_{xy} = -2\mathrm{Re}[\mu_1 U_1''(z_1) + \mu_2 U_2''(z_2)]$

in which prime (') denotes differentiation with respect to the parenthetical argument. It may be verified by differentiation that the displacement components corresponding to (26) are given by

$$u_x = 2\mathrm{Re}[p_1 U_1'(z_1) + p_2 U_2'(z_2)] \tag{27}$$

and $\quad u_y = 2\mathrm{Re}[q_1 U_1'(z_1) + q_2 U_2'(z_2)]$

provided

$$p_1 = a_{11}\mu_1^2 + a_{12} - a_{16}\mu_1 \quad , \quad p_2 = a_{11}\mu_2^2 + a_{12} - a_{16}\mu_2$$

$$\tag{28}$$

$$\text{and} \quad q_1 = a_{12}\mu_1 + \frac{a_{22}}{\mu_1} - a_{26} \quad , \quad q_2 = a_{12}\mu_2 + \frac{a_{22}}{\mu_2} - a_{26}$$

The U_1 and U_2 components of the stress function are taken to be half-power series, i.e.,

$$U_1''(z_1) = \sum_{n=1}^{\infty} C_n z_1^{\frac{n-2}{2}} \quad \text{and} \quad U_2''(z_2) = \sum_{n=1}^{\infty} D_n z_2^{\frac{n-2}{2}} \tag{29}$$

These will now be shown to satisfy boundary conditions appropriate to free crack faces by properly relating the complex coefficients C_n and D_n. From (26), the stresses corresponding to a typical term in (29) are

$$\sigma_x = 2\mathrm{Re}\left[\mu_1^2 C_n z_1^{\frac{n-2}{2}} + \mu_2^2 D_n z_2^{\frac{n-2}{2}}\right]$$

$$\sigma_y = 2\mathrm{Re}\left[C_n z_1^{\frac{n-2}{2}} + D_n z_2^{\frac{n-2}{2}}\right] \tag{30}$$

$$\text{and} \quad \tau_{xy} = -2\mathrm{Re}\left[\mu_1 C_n z_1^{\frac{n-2}{2}} + \mu_2 D_n z_2^{\frac{n-2}{2}}\right]$$

Upon considering the crack-tip neighborhood and coordinate system shown in figure 2, we can write

$$\sigma_y(x,0) = \tau_{xy}(x,0) = 0 \quad \text{for } x < 0 \tag{31}$$

11

as the crack-face boundary conditions. From (30), these require

$$\begin{array}{l}\text{Re}\\\text{Im}\end{array} (C_n + D_n) = 0 \qquad , \text{ when } n \text{ is } \begin{array}{l}\text{even}\\\text{odd}\end{array}$$

and

$$\begin{array}{l}\text{Re}\\\text{Im}\end{array} (\mu_1 C_n + \mu_2 D_n) = 0 \quad , \text{ when } n \text{ is } \begin{array}{l}\text{even}\\\text{odd}\end{array}$$

(32)

Equations (32) are satisfied if we set

$$C_n + D_n = (i)^{n+1} A_n$$

and

$$\mu_1 C_n + \mu_2 D_n = (i)^{n+1} B_n$$

(33)

in which i is the imaginary unit and A_n and B_n are arbitrary real constants. Using (33) to write C_n and D_n in terms of A_n and B_n, we obtain

$$C_n = (i)^{n+1} \frac{\mu_2 A_n - B_n}{\mu_2 - \mu_1}$$

and

$$D_n = (i)^{n+1} \frac{B_n - \mu_1 A_n}{\mu_2 - \mu_1}$$

(34)

From (26), (27), (29), and (34), we are now able to write the crack-tip stresses and displacements corresponding to a typical term in the U_1 and U_2 series.

$$\sigma_x = 2\text{Re}\left\{ \frac{(i)^{n+1}}{\mu_2 - \mu_1} \left[A_n \mu_1 \mu_2 \left(\mu_1 z_1^{\frac{n-2}{2}} - \mu_2 z_2^{\frac{n-2}{2}} \right) + B_n \left(\mu_2^2 z_2^{\frac{n-2}{2}} - \mu_1^2 z_1^{\frac{n-2}{2}} \right) \right] \right\}$$

$$\sigma_y = 2\text{Re}\left\{ \frac{(i)^{n+1}}{\mu_2 - \mu_1} \left[A_n \left(\mu_2 z_1^{\frac{n-2}{2}} - \mu_1 z_2^{\frac{n-2}{2}} \right) + B_n \left(z_2^{\frac{n-2}{2}} - z_1^{\frac{n-2}{2}} \right) \right] \right\}$$

(35)

and

$$\tau_{xy} = -2\text{Re}\left\{ \frac{(i)^{n+1}}{\mu_2 - \mu_1} \left[A_n \mu_1 \mu_2 \left(z_1^{\frac{n-2}{2}} - z_2^{\frac{n-2}{2}} \right) + B_n \left(\mu_2 z_2^{\frac{n-2}{2}} - \mu_1 z_1^{\frac{n-2}{2}} \right) \right] \right\}$$

$$\begin{array}{l}u_x\\ = \frac{4}{n}\text{Re}\left\{ \frac{(i)^{n+1}}{\mu_2 - \mu_1} \left[A_n \left(\mu_2 \frac{p_1}{q_1} z_1^{\frac{n}{2}} - \mu_1 \frac{p_2}{q_2} z_2^{\frac{n}{2}} \right) + B_n \left(\frac{p_2}{q_2} z_2^{\frac{n}{2}} - \frac{p_1}{q_1} z_1^{\frac{n}{2}} \right) \right] \right\}\\u_y\end{array}$$

(36)

12

$$\text{Repeated Roots } (\mu_1 = \mu_2 = \mu)$$

In this case the operators in (23) are not distinct; each is once repeated; i.e.,

$$D_\mu^2 \, D_{\bar\mu}^2 \, U(x,y) = 0 \tag{37}$$

where

$$D_\mu = \frac{\partial}{\partial y} - \mu \frac{\partial}{\partial x} \quad \text{and} \quad D_{\bar\mu} = \frac{\partial}{\partial y} - \bar\mu \frac{\partial}{\partial x} \tag{38}$$

Repeated integration now gives

$$U(x,y) = 2\mathrm{Re}[U_1(z_1) + \bar z_1 U_2(z_1)] \tag{39}$$

as the general real solution of (37). In (39),

$$z_1 = x + \mu y \quad \text{and} \quad \bar z_1 = x + \bar\mu y \tag{40}$$

Expressions for the stress components corresponding to (39) are found from (19) to be:

$$\sigma_x = 2\mathrm{Re}\,[\mu^2 U_1''(z_1) + 2\mu\bar\mu U_2'(z_1) + \mu^2 \bar z_1 U_2''(z_1)]$$

$$\sigma_y = 2\mathrm{Re}\,[U_1''(z_1) + 2U_2'(z_1) + \bar z_1 U_2''(z_1)] \tag{41}$$

and $\quad \tau_{xy} = -2\mathrm{Re}\,[\mu U_1''(z_1) + (\mu + \bar\mu) U_2'(z_1) + \mu\bar z_1 U_2''(z_1)]$

Moreover, the displacements,

$$u_x = 2\mathrm{Re}\,[p_1 U_1'(z_1) + p_2 U_2(z_1) + p_3 \bar z_1 U_2'(z_1)]$$

and $\quad u_y = 2\mathrm{Re}\,[q_1 U_1'(z_1) + q_2 U_2(z_1) + q_3 \bar z_1 U_2'(z_1)] \tag{42}$

can be shown* to be consistent with the stresses (41), the stress–strain equations (16) and the strain–displacement equations (14) provided

---

*In verifying (42) subject to (14), (16), (41), and (43) certain identities must be used appropriate to μ and $\bar\mu$ as repeated roots of (22). These are:

$$a_{16} = a_{11}(\mu + \bar\mu)$$
$$2a_{12} + a_{66} = a_{11}(\mu^2 + 4\mu\bar\mu + \bar\mu^2)$$
$$a_{26} = a_{11}\mu\bar\mu(\mu + \bar\mu)$$
and $\quad a_{22} = a_{11}\mu^2\bar\mu^2$

13

$$p_1 = p_3 = \mu^2 a_{11} + a_{12} - \mu a_{16}$$

$$p_2 = \mu(2\bar{\mu} - \mu) a_{11} + a_{12} - \bar{\mu} a_{16}$$

<div align="right">(43)</div>

$$q_1 = q_3 = a_{12}\mu + \frac{a_{22}}{\mu} - a_{26}$$

and
$$q_2 = a_{12}\bar{\mu} + \frac{a_{22}}{\mu}\left(2 - \frac{\bar{\mu}}{\mu}\right) - a_{26}$$

Again, to develop a half-power series analogous to (29), we take

$$U_1''(z_1) = \sum_{n=1}^{\infty} C_n z_1^{\frac{n-2}{2}} \qquad \text{and} \qquad U_2'(z_1) = \sum_{n=1}^{\infty} D_n z_1^{\frac{n-2}{2}}$$

<div align="right">(44)</div>

in which C_n and D_n are complex constants and n is anticipated to be a real integer. Following the same procedure used for the distinct-root case, we substitute (44) into (41) and consider crack-face boundary conditions (31). This leads to the requirement that C_n and D_n typically satisfy

$$C_n + \frac{n+2}{2} D_n = i^{n+1} A_n$$

<div align="right">(45)</div>

and
$$\mu C_n + \left(\bar{\mu} + \frac{n}{2}\mu\right) D_n = i^{n+1} B_n$$

in which A_n and B_n are real constants. The simultaneous solution of (45) for C_n and D_n yields

$$C_n = \frac{i^{n+1}}{\bar{\mu} - \mu}\left[\left(\bar{\mu} + \frac{n}{2}\mu\right) A_n - \frac{n+2}{2} B_n\right]$$

<div align="right">(46)</div>

and
$$D_n = \frac{i^{n+1}}{\bar{\mu} - \mu}(B_n - \mu A_n)$$

When these expressions are incorporated in (41) and (42), the following formulas for stresses and displacements evolve for a typical term of the series:

14

$$\sigma_x = \mathrm{Re}\left\{\frac{i^{n+1}}{\bar{\mu}-\mu}z_1^{\frac{n-2}{2}}\left[A_n\mu^2\left(n\mu-2\bar{\mu}-\mu(n-2)\frac{\bar{z}_1}{z_1}\right)\right.\right.$$

$$\left.\left.+B_n\mu\left(4\bar{\mu}-\mu(n+2)+\mu(n-2)\frac{\bar{z}_1}{z_1}\right)\right]\right\}$$

(47)

$$\sigma_y = \mathrm{Re}\left\{\frac{i^{n+1}}{\bar{\mu}-\mu}z_1^{\frac{n-2}{2}}\left[A_n\left(\mu(n-4)+2\bar{\mu}-\mu(n-2)\frac{\bar{z}_1}{z_1}\right).\right.\right.$$

$$\left.\left.+B_n\left((n-2)\left(\frac{\bar{z}_1}{z_1}-1\right)\right)\right]\right\}$$

$$\tau_{xy} = \mathrm{Re}\left\{\frac{i^{n+1}}{\bar{\mu}-\mu}z_1^{\frac{n-2}{2}}\left[\mu^2A_n(n-2)\left(\frac{\bar{z}_1}{z_1}-1\right)+B_n\left(n\mu-2\bar{\mu}-\mu(n-2)\frac{\bar{z}_1}{z_1}\right)\right]\right\}$$

and

$$u_x = \mathrm{Re}\left\{\frac{i^{n+1}}{\bar{\mu}-\mu}z_1^{\frac{n}{2}}\frac{2}{n}\left[A_n\left(p_1(2\bar{\mu}+n\mu)-2p_2\mu-np_1\mu\frac{\bar{z}_1}{z_1}\right)\right.\right.$$

$$\left.\left.+B_n\left(2p_2-p_1(n+2)+np_1\frac{\bar{z}_1}{z_1}\right)\right]\right\}$$

(48)

$$u_y = \mathrm{Re}\left\{\frac{i^{n+1}}{\bar{\mu}-\mu}z_1^{\frac{n}{2}}\frac{2}{n}\left[A_n\left(q_1(2\bar{\mu}+n\mu)-2q_2\mu-nq_1\mu\frac{\bar{z}_1}{z_1}\right)\right.\right.$$

$$\left.\left.+B_n\left(2q_2-q_1(n+2)+nq_1\frac{\bar{z}_1}{z_1}\right)\right]\right\}$$

The repeated-root case includes the stress and displacement functions appropriate to the crack-tip neighborhood in an isotropic material. For an isotropic material and plane stress conditions,

15

$$a_{11} = a_{22} = \frac{1}{E}$$

$$a_{12} = -\frac{\nu}{E}$$

$$a_{16} = a_{26} = 0 \qquad\qquad\qquad (49)$$

and $\quad a_{66} = \frac{2(1+\nu)}{E}$

With these simplifications, the characteristic polynomial (22) reduces to

$$\mu^4 + 2\mu^2 + 1 = 0 \qquad\qquad\qquad (50)$$

which has as a solution the repeated roots

$$\mu = \pm i \qquad\qquad\qquad (51)$$

Consequently,

$$U(x,y) = 2\,\mathrm{Re}\,[U_1(z) + \bar{z}U_2(z)] \qquad\qquad\qquad (52)$$

in which

$$z = x + iy \quad \text{and} \quad \bar{z} = x - iy \qquad\qquad\qquad (53)$$

Upon integrating (44)[†], we find

$$U_1(z) = C_n^* \, z^{\frac{n+2}{2}} \quad \text{and} \quad U_2(z) = D_n^* \, z^{\frac{n}{2}} \qquad\qquad\qquad (54)$$

as components of the isotropic form of $U(x,y)$. Combining (52) and (54), we find

$$U(x,y) = C_n^* \, z^{\frac{n+2}{2}} + \overline{C_n^*}\, \bar{z}^{\frac{n+2}{2}} + \bar{z}\, D_n^* \, z^{\frac{n}{2}} + z\, \overline{D_n^*}\, \bar{z}^{\frac{n}{2}} \qquad\qquad\qquad (55)$$

In polar form (see figure 2),

[†] In (54) it is convenient to use C_n^* and D_n^* to represent $4C_n/n(n+2)$ and $2D_n/n$, respectively.

16

$$z^{\frac{n}{2}} = r^{\frac{n}{2}} e^{i\frac{n\theta}{2}} = r^{\frac{n}{2}} \left(\cos \frac{n\theta}{2} + i \sin \frac{n\theta}{2} \right) \tag{56}$$

and
$$\bar{z}^{\frac{n}{2}} = r^{\frac{n}{2}} e^{-i\frac{n\theta}{2}} = r^{\frac{n}{2}} \left(\cos \frac{n\theta}{2} - i \sin \frac{n\theta}{2} \right)$$

so that (55) becomes

$$U(r, \theta) = C_n^* \, r^{\frac{n+2}{2}} \left(\cos \left(\frac{n}{2} + 1 \right) \theta + i \sin \left(\frac{n}{2} + 1 \right) \theta \right)$$

$$+ \overline{C_n^*} \, r^{\frac{n+2}{2}} \left(\cos \left(\frac{n}{2} + 1 \right) \theta - i \sin \left(\frac{n}{2} + 1 \right) \theta \right)$$

$$+ D_n^* \, r^{\frac{n+2}{2}} \left(\cos \left(\frac{n}{2} - 1 \right) \theta + i \sin \left(\frac{n}{2} - 1 \right) \theta \right)$$

$$+ \overline{D_n^*} \, r^{\frac{n+2}{2}} \left(\cos \left(\frac{n}{2} - 1 \right) \theta - i \sin \left(\frac{n}{2} - 1 \right) \theta \right)$$

$$= 2 r^{\frac{n+2}{2}} \left[\mathrm{Re}(C_n^*) \cos \left(\frac{n}{2} + 1 \right) \theta - \mathrm{Im}(C_n^*) \sin \left(\frac{n}{2} + 1 \right) \theta \right.$$

$$\left. + \mathrm{Re}(D_n^*) \cos \left(\frac{n}{2} - 1 \right) \theta - \mathrm{Im}(D_n^*) \sin \left(\frac{n}{2} - 1 \right) \theta \right] \tag{57}$$

which is a typical term in the familiar Williams series of stress functions appropriate to the crack–tip neighborhood in an isotropic material (ref. 14, 15). Imposition of the crack–face boundary conditions (31) leads to

$$\mathrm{Re}(D_n^*) = - \frac{\frac{n}{2} + 1}{\frac{n}{2} + (-1)^n} \, \mathrm{Re}(C_n^*)$$

$$\tag{58}$$

$$\mathrm{Im}(D_n^*) = - \frac{\frac{n}{2} + 1}{\frac{n}{2} - (-1)^n} \, \mathrm{Im}(C_n^*)$$

17

Upon substituting (58) into (57), we find the following expressions for stresses and displacements in polar form:

$$\sigma_r = \frac{1}{r}\frac{\partial U}{\partial r} + \frac{1}{r^2}\frac{\partial^2 U}{\partial \theta^2}$$

$$= \frac{1}{2}\,\text{Re}(C_n^*)\,r^{\frac{n-2}{2}}\,n\left[-(n+2)\cos\left(\frac{n+2}{2}\right)\theta + \frac{n+2}{n+2(-1)^n}(n-6)\cos\left(\frac{n-2}{2}\right)\theta\right]$$

$$+ \frac{1}{2}\,\text{Im}(C_n^*)\,r^{\frac{n-2}{2}}\,n\left[-(n+2)\sin\left(\frac{n+2}{2}\right)\theta + \frac{n+2}{n-2(-1)^n}(n-6)\sin\left(\frac{n-2}{2}\right)\theta\right]$$

$$\sigma_\theta = \frac{\partial^2 U}{\partial r^2}$$

$$= \frac{1}{2}\,\text{Re}(C_n^*)\,r^{\frac{n-2}{2}}\,n\left[(n+2)\cos\left(\frac{n+2}{2}\right) - \frac{n+2}{n+2(-1)^n}\cos\left(\frac{n-2}{2}\right)\theta\right] \tag{59}$$

$$+ \frac{1}{2}\,\text{Im}(C_n^*)\,r^{\frac{n-2}{2}}\,n(n+2)\left[\sin\left(\frac{n+2}{2}\right)\theta - \frac{n+2}{n-2(-1)^n}\sin\left(\frac{n-2}{2}\right)\theta\right]$$

$$\tau_{r\theta} = -\frac{\partial}{\partial r}\left(\frac{1}{r}\frac{\partial U}{\partial \theta}\right)$$

$$= \frac{1}{2}\,\text{Re}(C_n^*)\,r^{\frac{n-2}{2}}\,n\left[(n+2)\sin\left(\frac{n+2}{2}\right)\theta - \frac{n+2}{n+2(-1)^n}(n-2)\sin\left(\frac{n-2}{2}\right)\theta\right]$$

$$+ \frac{1}{2}\,\text{Im}(C_n^*)\,r^{\frac{n-2}{2}}\,n\left[-(n+2)\cos\left(\frac{n+2}{2}\right)\theta + \frac{n+2}{n-2(-1)^n}(n-2)\cos\left(\frac{n-2}{2}\right)\theta\right]$$

and

18

$$u_r = \frac{1+\nu}{E} \, \text{Re}(C_n^*) \, r^{\frac{n}{2}} \left[-(n+2) \cos\left(\frac{n+2}{2}\right)\theta - \frac{n+2}{n+2(-1)^n}\left(6 - \frac{8\nu}{1+\nu} - n\right) \cos\left(\frac{n-2}{2}\right)\theta \right]$$

$$- \frac{1+\nu}{E} \, \text{Im}(C_n^*) \, r^{\frac{n}{2}} \left[(n+2) \sin\left(\frac{n+2}{2}\right)\theta + \frac{n+2}{n-2(-1)^n}\left(6 - \frac{8\nu}{1+\nu} - n\right) \sin\left(\frac{n-2}{2}\right)\theta \right]$$

(60)

$$u_\theta = \frac{1+\nu}{E} \, \text{Re}(C_n^*) \, r^{\frac{n}{2}} \left[(n+2) \sin\left(\frac{n+2}{2}\right)\theta - \frac{n+2}{n+2(-1)^n}\left(6 - \frac{8\nu}{1+\nu} + n\right) \sin\left(\frac{n-2}{2}\right)\theta \right]$$

$$+ \frac{1+\nu}{E} \, \text{Im}(C_n^*) \, r^{\frac{n}{2}} \left[-(n+2) \cos\left(\frac{n+2}{2}\right)\theta + \frac{n+2}{n-2(-1)^n}\left(6 - \frac{8\nu}{1+\nu} + n\right) \cos\left(\frac{n-2}{2}\right)\theta \right]$$

FORMULATION OF CRACKED ELEMENT STIFFNESS MATRICES

Two types of cracked elements, as shown in figure 3, have been developed and implemented, because many fracture mechanics problems are symmetric about the plane of the crack. One formulation takes only the symmetric terms in the series solution and, hence, is applicable only to symmetric problems ($K_{II} = 0$); the other formulation makes use of both symmetric and anti-symmetric terms and is applicable to unsymmetric or mixed-mode problems (K_I and K_{II}).

The coordinate system of an 8-node symmetric element has its origin at the crack tip. It is rectangular in shape with a three-to-one aspect ratio. Placement of the nodes relative to the rectangle is pre-determined with a node at each corner plus nodes at the one-third points of each of the long sides. The lower side (nodes 6, 7, 8, and 1) is coincident with the crack direction and presumed axis of symmetry. Nodes 6 and 7 are on the free crack face. Nodes 8 and 1 are on the prolongation of the crack. They are constrained rigidly as to vertical displacement and are free of shear forces – conditions that are consistent with symmetry.

The 8-node symmetric element has 16 displacement degrees of freedom, two per node corresponding to the in-plane displacement components. Thus, it incorporates the first 13 symmetric terms of the series associated with rigid-body motion in the plane. These 13 coefficients and the three rigid-body parameters are referred to as the 16 generalized co-ordinates of the cracked element. The stresses and displacements corresponding to these 16 generalized coordinates are evaluated on the boundary of the element. Products of stress and displacement contributing to boundary work are performed and integrated. The result is a homogenous quadratic form in the generalized coordinates, and the coefficient of each term is an element of the cracked element stiffness matrix with respect to the generalized coordinates. Once the stiffness matrix with respect to generalized coordinates is deter-mined, the stiffness matrix with respect to nodal displacements is formed using the series (with rigid-body terms) to write nodal displacements in terms of the generalized coordinates.

The 10-node unsymmetric cracked element as shown in figure 3 is square with equally spaced nodes around its boundary. Like the symmetric cracked element, the shape of the element and relative location of the nodes were chosen to provide modeling convenience. The generalized coordinates correspond to the first 9 symmetric terms and first 8 anti-sym-metric terms of the series, plus the 3 rigid-body displacement parameters. The stiffness matrix was again generated by integration around the boundary.

To formulate the cracked-element stiffness matrix, it is convenient to introduce dimensionless variables for both anisotropic and isotropic cases.

Anisotropic Case

The dimensionless variables for the anisotropic case are given as

$$Z_1 = z_1/\Delta, \qquad\qquad Z_2 = z_2/\Delta$$

$$P_1 = p_1/a_{11}, \qquad\qquad P_2 = p_2/a_{11}$$

$$Q_1 = q_1/a_{11}, \qquad\qquad Q_2 = q_2/a_{11}$$

$$C_n = a_{11} \Delta^{\frac{n}{2}-1} A_n, \qquad D_n = a_{11} \Delta^{\frac{n}{2}-1} B_n$$

$$S_x = a_{11}\sigma_x, \qquad\qquad S_y = a_{11}\sigma_y, \qquad\qquad S_{xy} = a_{11}\tau_{xy}$$

$$U_x = u_x/\Delta \qquad\qquad U_y = u_y/\Delta$$

(61)

where Δ is a characteristic length and is taken to be the distance between nodes on the cracked element. In terms of the dimensionless variables in equation (61), equations (35) and (36) take the form below

$$S_x = 2\mathrm{Re}\left\{\frac{(i)^{n+1}}{\mu_2 - \mu_1}\left[C_n \mu_1 \mu_2 \left(\mu_1 Z_1^{\frac{n-2}{2}} - \mu_2 Z_2^{\frac{n-2}{2}}\right)\right.\right.$$

$$\left.\left. + D_n\left(\mu_2^2 Z_2^{\frac{n-2}{2}} - \mu_1^2 Z_1^{\frac{n-2}{2}}\right)\right]\right\}$$

$$S_y = 2\mathrm{Re}\left\{\frac{(i)^{n+1}}{\mu_2 - \mu_1}\left[C_n\left(\mu_2 Z_1^{\frac{n-2}{2}} - \mu_1 Z_2^{\frac{n-2}{2}}\right)\right.\right.$$

$$\left.\left. + D_n\left(Z_2^{\frac{n-2}{2}} - Z_1^{\frac{n-2}{2}}\right)\right]\right\}$$

(62)

$$S_{xy} = -2\mathrm{Re}\left\{\frac{(i)^{n+1}}{\mu_2 - \mu_1}\left[C_n \mu_1 \mu_2\left(Z_1^{\frac{n-2}{2}} - Z_2^{\frac{n-2}{2}}\right)\right.\right.$$

$$\left.\left. + D_n\left(\mu_2 Z_2^{\frac{n-2}{2}} - \mu_1 Z_1^{\frac{n-2}{2}}\right)\right]\right\}$$

and

$$\begin{Bmatrix} U_x \\ U_y \end{Bmatrix} = \frac{4}{n} \operatorname{Re} \left\{ \frac{(i)^{n+1}}{\mu_2 - \mu_1} \left[C_n \left(\mu_2 \frac{P_1}{Q_1} z_1^{\frac{n}{2}} - \mu_1 \frac{P_2}{Q_2} z_2^{\frac{n}{2}} \right) \right.\right.$$
$$\left.\left. + D_n \left(\frac{P_2}{Q_2} z_2^{\frac{n}{2}} - \frac{P_1}{Q_1} z_1^{\frac{n}{2}} \right) \right] \right\} \tag{63}$$

Equations (62) and (63) are the basic equations needed to form the stiffness matrix of the anisotropic cracked element. The strain energy V stored in the cracked element can be computed by numerically integrating the work of the surface tractions around the boundary. This yields

$$2V = \frac{h\Delta^2}{a_{11}} q^T k q \tag{64}$$

in which $h = $ the uniform thickness of the cracked element

$q = $ the column matrix of generalized coordinates

$q^T = $ the transpose of q

$k = $ the stiffness matrix with respect to generalized coordinates

Let D denote the column of dimensionless nodal displacement components in the elemental cartesian coordinate system. The matrix C in

$$D = Cq \tag{65}$$

is obtained by evaluating equations (63) at the nodes. The inverse of C may be found numerically with the result

$$q = C^{-1} D \tag{66}$$

Thus, from (64),

$$2V = D^T (C^{-1})^T \frac{h\Delta^2}{a_{11}} k \, C^{-1} D \tag{67}$$

or in terms of D^*, the column of dimensional nodal displacements

$$2V = D*^T (C^{-1})^T \frac{h}{a_{11}} k\, C^{-1}\, D* \tag{68}$$

So

$$K = \frac{h}{a_{11}} (C^{-1})^T k\, C^{-1} \tag{69}$$

Once the stiffness matrix of the cracked element is formed, its incorporation into the stiffness matrix of an assembly follows exactly the procedure used for conventional elements. The same approach was followed for the case of repeated roots.

Isotropic Case

The dimensionless variables introduced for an isotropic case are given below:

$$R = \frac{r}{\Delta}, \qquad U_R = \frac{u_r}{\Delta}, \qquad U_\theta = \frac{u_\theta}{\Delta}$$

$$S_R = \frac{\sigma_r}{G}, \qquad S_\theta = \frac{\sigma_\theta}{G}, \qquad S_{R\theta} = \frac{\tau_{r\theta}}{G}$$

$$s_n^* = \frac{\Delta^{\frac{n}{2}-1}}{2G}\, \mathrm{Re}\,(C_n^*)$$

$$a_n^* = -\frac{\Delta^{\frac{n}{2}-1}}{2G}\, \frac{n+2}{n-2\,(-1)^n}\, \mathrm{Im}\,(C_n^*) \tag{70}$$

where Δ is also a characteristic length as defined before.

In terms of the dimensionless variables in equation (70), equations (59) and (60) take the following form:

$$S_R(R, \theta) = \sum_{n=1}^{\infty} n R^{\frac{n}{2}-1} \left\{ s_n^* \left[-(n+2)\cos\left(\frac{n}{2}+1\right)\theta + f(n)(n-6)\cos\left(\frac{n}{2}-1\right)\theta \right] \right.$$

$$\left. + a_n^* \left[g(n)(n+2)\sin\left(\frac{n}{2}+1\right)\theta - (n-6)\sin\left(\frac{n}{2}-1\right)\theta \right] \right\}$$

23

$$S_{\theta}(R, \theta) = \sum_{n=1}^{\infty} n(n+2) R^{\frac{n}{2}-1} \left\{ s_n^* \left[\cos\left(\frac{n}{2}+1\right)\theta - f(n) \cos\left(\frac{n}{2}-1\right)\theta \right] \right.$$

$$\left. + a_n^* \left[-g(n) \sin\left(\frac{n}{2}+1\right)\theta + \sin\left(\frac{n}{2}-1\right)\theta \right] \right\}$$

(71)

$$S_{R\theta}(R, \theta) = \sum_{n=1}^{\infty} n R^{\frac{n}{2}-1} \left\{ s_n^* \left[(n+2) \sin\left(\frac{n}{2}+1\right)\theta - f(n)(n-2) \sin\left(\frac{n}{2}-1\right)\theta \right] \right.$$

$$\left. + a_n^* \left[g(n)(n+2) \cos\left(\frac{n}{2}+1\right)\theta - (n-2) \cos\left(\frac{n}{2}-1\right)\theta \right] \right\}$$

$$U_R(R, \theta) = \sum_{n=1}^{\infty} R^{\frac{n}{2}} \left\{ s_n^* \left[-(n+2) \cos\left(\frac{n}{2}+1\right)\theta - f(n)(6-8\xi-n) \cos\left(\frac{n}{2}-1\right)\theta \right] \right.$$

$$\left. + a_n^* \left[(n+2) g(n) \sin\left(\frac{n}{2}+1\right)\theta + (6-8\xi-n) \sin\left(\frac{n}{2}-1\right)\theta \right] \right\}$$

(72)

$$U_{\theta}(R, \theta) = \sum_{n=1}^{\infty} R^{\frac{n}{2}} \left\{ s_n^* \left[(n+2) \sin\left(\frac{n}{2}+1\right)\theta - f(n)(6-8\xi+n) \sin\left(\frac{n}{2}-1\right)\theta \right] \right.$$

$$\left. + a_n^* \left[(n+2) g(n) \cos\left(\frac{n}{2}+1\right)\theta - (6-8\xi+n) \cos\left(\frac{n}{2}-1\right)\theta \right] \right\}$$

in which

$$f(n) = \frac{\frac{n}{2}+1}{\frac{n}{2}+(-1)^n} \qquad g(n) = \frac{\frac{n}{2}-(-1)^n}{\frac{n}{2}+1}$$

(73)

$$\xi = \begin{cases} \nu & \text{for plane strain} \\ \dfrac{\nu}{1+\nu} & \text{for plane stress} \end{cases}$$

24

Equations (71) and (72) are the basic equations needed to form the stiffness matrix of the isotropic cracked element.

It is noticed that equations (72) for the displacement components have been written so as to keep the parts independent of ξ and distinct from the parts dependent on ξ. This distinction was made to permit the storage of the stiffness matrix as the sum of two matrices that are each internally independent of material parameters.

By numerical integration, the strain energy V stored in the cracked element can be written in terms of the stiffness matrices k_1 and k_2, i.e.,

$$2V = Gh\Delta^2 q^T (k_1 + \xi k_2) q \tag{74}$$

in which h is the uniform thickness of the element. Following the same approach as for the anisotropic case, equation (74) can also be written in terms of D^*, the column matrix of dimensional nodal displacements,

$$2V = D^{*T} (C^{-1})^T Gh (k_1 + \xi k_2) C^{-1} D^* \tag{75}$$

So that

$$K = Gh (C^{-1})^T (k_1 + \xi k_2) C^{-1} \tag{76}$$

Each of the stiffness matrices of these isotropic cracked elements is stored as the sum of two matrices that are independent of the size and material properties of the cracked element. This means that the boundary integration mentioned previously does not have to be repeated for each application. Consequently, the efficiency of the analysis program in conventional finite-element applications is not diminished at all by the addition of the cracked element. The displacement incompatibility that exists between nodes where the cracked element interfaces with a conventional element seems inconsequential in light of the exceptional accuracy obtained in many and varied applications, including the sample problems.

STRESS–INTENSITY FACTORS AND STRAIN–ENERGY RELEASE RATES

Stress–Intensity Factors

The leading terms in equations (35) and (59) contain the singularity $r^{-1/2}$; all subsequent terms are non-singular. The coefficients A_1 and B_1 ($C_1{}^*$ for isotropic case) are related to the opening and sliding mode stress-intensity factors K_I and K_{II} by the following formulas:

Anisotropic Case:

$$K_I = \lim_{x \to o} \sqrt{2\pi x} \ \sigma_y(x, o) = -2\sqrt{2\pi} \ A_1$$

$$K_{II} = \lim_{x \to o} \sqrt{2\pi x} \ \tau_{xy}(x, o) = 2\sqrt{2\pi} \ B_1$$

(77)

Isotropic Case:

$$K_I = \lim_{r \to o} \sqrt{2\pi r} \ \sigma_\theta(r, o) = 6\sqrt{2\pi} \ \text{Re}\ (C_1{}^*)$$

$$K_{II} = \lim_{r \to o} \sqrt{2\pi r} \ \tau_{r\theta}(r, o) = -2\sqrt{2\pi} \ \text{Im}\ (C_1{}^*)$$

(78)

Strain–Energy Release Rates

The strain-energy release rates are related to the stress-intensity factors by the elastic coefficients in the following fashion:

$$G_i = cK_i{}^2 \qquad i = I, II$$

(79)

where "i" indicates the mode number. The total strain-energy release rate is the summation of energy rate at each mode based upon linear superposition. The elastic coefficients c that relate energy rates to stress-intensity factors are listed in Table I.

TABLE I

ELASTIC COEFFICIENTS RELATING ENERGY RATES TO STRESS-INTENSITY FACTORS
(Reference 16)

MATERIAL	CONDITION	ELASTIC COEFFICIENTS	
		MODE I	MODE II
Isotropic	Plane-Strain	$\dfrac{(1-\nu^2)}{E}$	$\dfrac{(1-\nu^2)}{E}$
	Plane-Stress	$\dfrac{1}{E}$	$\dfrac{1}{E}$
Orthotropic	Plane-Strain	$\left(\dfrac{\overline{a_{11}}\,\overline{a_{22}}}{2}\right)^{1/2}\left[\dfrac{\overline{a_{22}}}{\overline{a_{11}}}+\dfrac{2\overline{a_{12}}+\overline{a_{66}}}{2\overline{a_{11}}}\right]^{1/2}$	$\dfrac{\overline{a_{11}}}{2}\left[\dfrac{\overline{a_{22}}}{\overline{a_{11}}}+\dfrac{2\overline{a_{12}}+\overline{a_{66}}}{2\overline{a_{11}}}\right]^{1/2}$
	Plane-Stress	$\left(\dfrac{a_{11}\,a_{22}}{2}\right)^{1/2}\left[\dfrac{a_{22}}{a_{11}}+\dfrac{2a_{12}+a_{66}}{2a_{11}}\right]^{1/2}$	$\dfrac{a_{11}}{2}\left[\dfrac{a_{22}}{a_{11}}+\dfrac{2a_{12}+a_{66}}{2a_{11}}\right]^{1/2}$
Anisotropic	Plane-Strain	$\dfrac{1}{2}\,\text{Im}\left[-\overline{a_{22}}\dfrac{\mu_1+\mu_2}{\mu_1\mu_2}\right]$	$\dfrac{1}{2}\,\text{Im}\left[\overline{a_{11}}(\mu_1+\mu_2)\right]$
	Plane-Stress	$\dfrac{1}{2}\,\text{Im}\left[-a_{22}\dfrac{\mu_1+\mu_2}{\mu_1\mu_2}\right]$	$\dfrac{1}{2}\,\text{Im}\left[a_{11}(\mu_1+\mu_2)\right]$

BRIEF DESCRIPTION OF CRACKED ELEMENT COMPUTER PROGRAM

The computer program is an all-FORTRAN program which uses only conventional I/O (FORTRAN READ and WRITE statements) and the standard library routines. It contains the following finite elements:

- Axial element
- Linear spring element
- Plane-stress/strain, isotropic and anisotropic, triangular element
- Eight-node symmetric isotropic cracked element
- Eight-node symmetric anisotropic cracked element
- Ten-node unsymmetric isotropic cracked element
- Ten-node unsymmetric anisotropic cracked element

The computer program consists of a main program called CRAK, which allocates the core and calls sequentially four main driver subroutines (INPUT, KFORM, CHOL, OUTPUT), and 32 subroutines. These subroutines have been overlayed to reduce the core required for program code, permanent data, and program table. The segment structure of the program is shown in figure 4. The name and function of each subroutine are given in Table II.

The input segment of the program contains data generator features to minimize the labor required to input a model. During the input sequence, a banding algorithm is used to resequence the node numbers to minimize the band-width of the structural stiffness matrix which is assembled in the KFORM segment. This banding algorithm is quite effective and helps to minimize execution times. A banded Cholesky decomposition procedure (segment CHOL) is used to solve the system of equations. The computer program organization is especially characterized by its flexibility of application. The planned segmented structure of the program also makes it easy to insert additional cracked and conventional elements as desired.

The scheme of the analysis is basically divided into the following stages:

- Input of geometry, material data and restraints
- Input of applied nodal loads and imposed nodal displacements
- Calculation of element stiffness matrices
- Assembly of element stiffness into a system stiffness
- Solution of simultaneous equations for nodal displacements
- Output nodal displacements

- Calculation and output of forces (or stresses) in conventional elements

- Calculation and output of stress-intensity factors and strain-energy release rates

The overall logic flow of the computer program is depicted in figure 5.

The computer program is efficient in its use of computing time and core storage. Core use can easily be changed to fit individual problem sizes if desired. Full advantage has been taken of symmetry and the banded nature of the simultaneous equations to be solved, and no data are generated when not required.

TABLE II

FUNCTION OF SUBROUTINES

SUBROUTINE NAME	FUNCTION
INPUT	Inputs model general specifications
CORIN	Inputs nadal coordinates and restraints
TRIN	Inputs triangular elements for both isotropic and anisotropic cases
SPRGIN	Inputs spring elements
AXIN	Inputs axial elements
CRKIN8	Inputs 8-node symmetric cracked elements for both isotropic and anisotropic cases
CRKN10	Inputs 10-node unsymmetric cracked elements for both isotropic and anisotropic cases.
MATIN	Inputs material properties
DISPIN	Inputs imposed displacements
LOADIN	Inputs applied loads
CONNEC	Generates data which subroutine BANDIT requires
BANDIT	Renumbers the node points to minimize band width
BAND	Determines the band-width
KFORM	Forms a complete stiffness matrix
TRI	Computes triangular element stiffness matrix
SPRNG	Computes spring element stiffness matrix
AXI	Computes axial element stiffness matrix
CRAK8	Switches control to either CRAK8I or CRAK8A

TABLE II   (Continued)

FUNCTION OF SUBROUTINES

SUBROUTINE NAME	FUNCTION
CRAK8I	Computes stiffness matrix for 8-node symmetric isotropic cracked element
CRAK8A	Computes stiffness matrix for 8-node symmetric anisotropic cracked element
CRAK10	Switches control to either CRK10I or CRK10A
CRK10I	Computes stiffness matrix for 10-node unsymmetric isotropic cracked element
CRK10A	Computes stiffness matrix for 10-node unsymmetric anisotropic cracked element
INVERT	Inverts a matrix
CPLXRT	Computes complex roots of a specified 4th order characteristic polynomial
CPWR	Raises complex number to a real power
THCOEF	Transforms thermal coefficients from one reference axis to another
THDISP	Computes thermal displacements for both symmetric and unsymmetric cracked element
CHOL	Solves simultaneous equations
OUTPUT	Controls output data
DISPOT	Outputs Displacements
TRIOUT	Calculates triangular elements output
SPROUT	Calculates spring elements output
AXIOUT	Calculates axial elements output

TABLE II   (Continued)

FUNCTION OF SUBROUTINES

SUBROUTINE NAME	FUNCTION
CRKO8	Calculates K_I for the 8-node symmetric elements
CRKO10	Calculates K_I and K_{II} for the 10-node unsymmetric elements

SAMPLE PROBLEMS

This finite-element computer program has been tested extensively. Both symmetric and unsymmetric cracked elements have performed well with respect to accuracy and efficiency, as shown by sample problems presented here. These results were achieved with a relatively coarse finite-element grid. With refinements in the grid, even more accurate results would be obtained. The symmetric cracked element normally gives more accurate results than the unsymmetric cracked element, which is understandable in view of the fact that the unsymmetric cracked element has fewer degrees of freedom that it can bring to bear on the first mode. However, the unsymmetric cracked element can be used in a much wider class of crack problems and is more practical for industrial applications.

To illustrate the capabilities of these two types of crack elements (symmetric and unsymmetric), a number of selected sample problems are included in this report. These sample problems were chosen to demonstrate (1) the accuracy and economy of the elements, and (2) the versatilities of the elements to perform analyses for structural configurations of practical importance.

Anisotropic Case

Center-Cracked and Double-Edge-Cracked Orthotropic Tension Plates – A center-cracked and/or a double-edge-cracked orthotropic plate (Figure 6) subjected to uniform tension as solved by Snyder and Cruse (ref. 17) was investigated. The plate analyzed is 228.6 mm long and 76.2 mm wide. The finite-element models used for both the center-cracked plate and the double-edge-cracked plate are shown in figure 7. The half-crack lengths, a, analyzed are 15.24 mm and 22.86 mm for the center-cracked plate and 15.24 mm only for the double-edge-cracked plate.

Numerical results were obtained for 10 representative graphite fiber-reinforced epoxy laminates: $(0)_s$, $(\pm 30)_s$, $(\pm 34)_s$, $(\pm 45)_s$, $(\pm 56)_s$, $(\pm 60)_s$, $(90)_s$, $(90_4/\pm 45)_s$, $(90_2/\pm 45)_s$, $(0/\pm 45/90)_s$. Lamina properties used were:

$$E_{11} = 144.795 \text{ GPa} \quad , \quad G_{12} = 9.653 \text{ GPa}$$

$$E_{22} = 11.722 \text{ GPa} \quad , \quad \nu_{12} = 0.21$$

Table III indicates the complex roots obtained from the characteristic equation for each laminate.

Results are presented in Tables IV, V, and VI. The distribution of differences from Snyder and Cruse's results are summarized in table VII. Notice that the results generated using 8-node symmetric cracked element are closer to Snyder and Cruse's results than those

33

TABLE III

COMPLEX ROOTS OF CHARACTERISTIC EQUATION

MATERIAL	μ_1		μ_2	
	α_1	β_1	α_2	β_2
$(0/\pm 45/90)_S$	0.	0.9999	0.	1.0001
$(90_2/\pm 45)_S$	0.2680	0.7007	-0.2680	0.7007
$(90_4/\pm 45)_S$	0.	0.5554	0.	0.8372
$(90)_S$	0.	0.2704	0.	1.0522
$(\pm 45)_S$	0.7763	0.6304	-0.7763	0.6304
$(\pm 30)_S$	0.9648	1.0090	-0.9648	1.0090
$(\pm 60)_S$	0.4951	0.5177	-0.4951	0.5177
$(0)_S$	0.	0.9504	0.	3.6982
$(\pm 34)_S$	0.9415	0.8730	-0.9415	0.8730
$(\pm 56)_S$	0.5711	0.5296	-0.5711	0.5296

NOTE: $\mu_j = \alpha_j + \beta_j i$, where $i = \sqrt{-1}$, $j = 1, 2$

TABLE IV

STRESS-INTENSITY FACTORS OF
CENTER-CRACKED PLATES (a = 15.24 mm, a/w = 0.4)

MATERIAL	SNYDER & CRUSE K_I (MPa - $\sqrt{m}$)	8-NODE CRACKED ELEMENT		10-NODE CRACKED ELEMENT	
		K_I	% OFF	K_I	% OFF
$(0/\pm 45/90)_S$	1.670	1.675	+0.32	1.622	-2.88
$(90_2/\pm 45)_S$	1.679	1.696	+1.01	1.652	-1.61
$(90_4/\pm 45)_S$	1.670	1.702	+1.92	1.671	+0.06
$(90)_S$	1.683	1.669	-0.83	1.755	+4.28
$(\pm 45)_S$	1.745	1.634	-6.36	1.617	-7.34
$(\pm 30)_S$	1.712	1.643	-4.03	1.574	-8.06
$(\pm 60)_S$	1.719	1.683	-2.09	1.649	-4.07
$(0)_S$	1.645	1.652	+0.43	1.578	-4.07

TABLE V

STRESS-INTENSITY FACTORS OF
CENTER-CRACKED PLATES (a = 22.86 mm, a/w = 0.6)

MATERIAL	SNYDER & CRUSE K_I (MPa $-\sqrt{m}$)	8-NODE CRACKED ELEMENT		10-NODE CRACKED ELEMENT	
		K_I	% OFF	K_I	% OFF
$(0/\pm 45/90)_S$	2.396	2.396	+0.01	2.326	-2.92
$(90_2/\pm 45)_S$	2.422	2.444	+0.91	2.389	-1.36
$(90_4/\pm 45)_S$	2.396	2.446	+2.09	2.413	+0.71
$(90)_S$	2.394	2.419	+1.04	2.574	+7.52
$(\pm 45)_S$	2.599	2.421	-6.85	2.393	-7.93
$(\pm 30)_S$	2.518	2.405	-4.49	2.302	-8.58
$(\pm 60)_S$	2.533	2.473	-2.37	2.430	-4.07
$(0)_S$	2.314	2.336	+0.95	2.229	-3.67

TABLE VI

STRESS-INTENSITY FACTORS OF
DOUBLE-EDGE-CRACKED PLATES (a = 15.24 mm, a/w = 0.4)

MATERIAL	SNYDER & CRUSE K_I (MPa $-\sqrt{m}$)	8-NODE CRACKED ELEMENT		10-NODE CRACKED ELEMENT	
		K_I	% OFF	K_I	% OFF
$(0/\pm 45/90)_S$	1.722	1.701	-1.22	1.649	-4.24
$(90_2/\pm 45)_S$	1.722	1.729	+0.41	1.685	-2.15
$(90_4/\pm 45)_S$	1.706	1.725	+1.11	1.688	-1.06
$(90)_S$	1.709	1.689	-1.17	1.752	+2.52
$(\pm 45)_S$	1.700	1.757	+3.35	1.766	+3.88
$(\pm 30)_S$	1.783.	1.722	-3.42	1.697	-4.82
$(\pm 60)_S$	1.717	1.767	+2.91	1.736	+1.11
$(0)_S$	1.670	1.660	-0.60	1.598	-4.31
$(\pm 34)_S$	1.750	1.737	-0.74	1.724	-1.49
$(\pm 56)_S$	1.745	1.765	+1.15	1.746	+0.06

TABLE VII

DIFFERENCES FROM SNYDER AND CRUSE'S RESULTS

TYPE OF PLATE	TOTAL NUMBER OF PROBLEMS	DISTRIBUTION OF DISCREPANCY		
		DIFFERENCE (%)	NO. OF PROBLEMS	
			8-NODE CRACKED EL.	10-NODE CRACKED EL.
CENTER–CRACKED (a = 15.24mm, a/w = 0.4)	8	0 - ±3	6	3
		±3 - ±5	1	3
		±5 - ±7	1	0
		±7 - ±9	0	2
CENTER-CRACKED (a = 22.86 mm, a/w = 0.6)	8	0 - ±3	6	3
		±3 - ±5	1	2
		±5 - ±7	1	0
		±7 - ±9	0	3
DOUBLE-EDGE-CRACKED (a = 15.24 mm, a/w = 0.4)	10	0 - ±3	8	6
		±3 - ±5	2	4
		±5 - ±7	0	0
		±7 - ±9	0	0

obtained from the 10-node unsymmetric cracked element. Since Snyder and Cruse used the boundary-integral approach, no definite conclusion can be drawn with regard to the absolute accuracy of their results. Besides, these finite-element solutions used a large integration step size (10 steps between nodes) along the boundaries for the numerical integration in forming the stiffness matrix of the cracked element. Accuracy would be improved by reducing the integration step size (increasing the number of steps between nodes).

Longitudinally Cracked Orthotropic Strip- The longitudinally cracked orthotropic strip problem as shown in figure 8 was solved under plane-stress and imposed displacement conditions. An analytical solution was developed based upon the energy equivalence and Sih's results of ref. 18. The solution is given below as

$$K_I{}^2 = \frac{\frac{1}{2}\left(\frac{a_{11}}{a_{11}\,a_{22} - a_{12}{}^2}\right)\frac{\delta^2}{h}}{\frac{a_{11}\,a_{22}}{2}\left[\sqrt{\frac{a_{22}}{a_{11}}} + \frac{2a_{12} + a_{66}}{2a_{11}}\right]^{1/2}} \tag{80}$$

where a_{ij} = Elements of the material compliance matrix

δ = Imposed displacement

h   = Height of the plate

Numerical results were obtained for the two different laminates shown in table VIII. In one case, the laminate is stiffer in the direction normal to the crack. In the other case, the laminate is stiffer in the direction of the crack. Both laminate cases were solved using a single cracked element and the two different model representations shown in figure 9. The results are summarized in table IX.

45-Degree Cracked Finite Orthotropic Plate – This problem is shown in figure 10. The finite-element model (figure 11) representing this plate consists of 130 nodes, 210 anisotropic triangular elements, and two 10-node anisotropic cracked elements. The problem was solved under uniform remote stress and plane-stress conditions. The stress-intensity factors obtained are given below:

$$K_I = 1.1376 \times 10^{-3} \text{ MPa} - \sqrt{m} \qquad \text{and} \qquad K_{II} = 1.1784 \times 10^{-3} \text{ MPa} - \sqrt{m}$$

Both K_I and K_{II} are within ± 2 percent (-1.77% and +1.75%, respectively) of Sih's solution, ref. 18, (K_I and K_{II} = 1.1581 $\times 10^{-3}$ MPa $- \sqrt{m}$) for an infinite sheet, and they satisfy NASA's requirement for the accuracy of the program.

TABLE VIII

LAMINATE STIFFNESS MATRICES (Scotchply 1002)

LAMINATE I	LAMINATE II
$[A] =$ (GPa) $\begin{bmatrix} 11.500 & 0.572 & 0 \\ 0.572 & 34.503 & 0 \\ 0 & 0 & 4.854 \end{bmatrix}$	$[A] =$ (GPa) $\begin{bmatrix} 34.503 & 0.572 & 0 \\ 0.572 & 11.500 & 0 \\ 0 & 0 & 4.854 \end{bmatrix}$

NOTE: $\{\sigma\}_{x-y} = [A] \{\epsilon\}_{x-y}$, where x-y refers to the reference coordinates

TABLE IX

SUMMARY OF RESULTS FOR A LONGITUDINALLY
CRACKED ORTHOTROPIC STRIP

METHOD	LAMINATE I		LAMINATE II	
	K_I $(MPa-\sqrt{m})$	ERROR %	K_I $(MPa-\sqrt{m})$	ERROR %
Analytical Solution Ref. (18)	12.477	-	5.474	-
1 Cracked Element	13.845	10.96	5.515	0.75
1 Cracked Element & 8 Triangular Elements	13.527	8.42	5.527	0.97
1 Cracked Element & 117 Triangular Elements	12.474	-0.02	5.326	-2.70

Isotropic Case

Cracked Tension Plates - The sample problem, shown in figure 12, was the first problem analyzed with the symmetric cracked element. It exhibits the degree of accuracy which has been consistently achieved in numerous subsequent problems. The finite-element model has 30 nodes, 35 triangular elements, and one 8-node symmetric cracked element. The three configurations (the single-edge crack, the double-edge crack, and the center-crack) were all individually analyzed with this one model for an a/w ratio of 1/3. The model grid, which is quite coarse, results in the single-edge-crack model having 57 displacement degrees-of-freedom (DOF), while the double-edge-crack and center-crack models have 51 DOF. The stress-intensity factors computed using these configurations are compared with ASTM (American Society for Testing and Materials) values. The accuracy of the finite-element predictions are impressive (<1.5% error) for all three cases. Refinements in the model would produce steady convergence toward ASTM values.

The same cracked problems were solved using an unsymmetric cracked element. The finite-element model as shown in figure 13 consists of 54 nodes, 69 triangular elements, and one 10-node unsymmetric cracked element. The results are not as good as those obtained using the 8-node symmetric cracked element, because the 8-node element has more degrees of freedom to bear on the first node.

An eccentric crack problem as shown in figure 14 was also solved, and the results compared with Isida's solution.

All these results are summarized in table X for reference.

Bi-Material Cracked Plate - This problem, as shown in figure 15, was solved in response to the NASA's Request for Proposal (RFP 1-31-4957), dated 28 May 1974. It was required that the stress-intensity factors of this isotropic, generalized plane-strain problem must be within $\pm2\%$ of Erdogan's results for an infinite plate (ref. 19). All dimensions and material properties are given in figure 15.

In the finite-element model shown in figure 16, only the upper half of the plate has been modeled due to its symmetry with respect to the x-axis. It contains 100 nodes, 148 plane-strain triangles, and 2 eight-node symmetric cracked elements.

A uniform displacement of 46.228×10^{-6} mm was imposed on the top boundary nodes. This was arrived at as follows. For plane strain,

$$\delta = \frac{H(1 - \nu_1^2) \, S_1}{E_1} = \frac{H(1 - \nu_2^2) \, S_2}{E_2} \tag{81}$$

where H is the half-height of the finite sheet. S_1 was taken as unity.

TABLE X

SUMMARY OF TYPICAL RESULTS FOR ISOTROPIC TENSION PANELS

CRACK DESCRIPTION	EIGHT-NODE SYMMETRIC ELEMENT (ESE)		TEN-NODE UNSYMMETRIC ELEMENT (TUE)	
	F. E. MODEL	K_I % ERROR	F. E. MODEL	K_I % ERROR
SINGLE EDGE CRACK (a/W = 1/3)	35 TRIANGULAR ELEMENTS PLUS	-1.2	68 TRIANGULAR ELEMENTS PLUS	-2.6
DOUBLE EDGE CRACK (a/W = 1/3)	1 ESE,	-1.5	1 TUE,	-2.6
CENTER CRACK (a/W = 1/3)	DOF = 57	+0.15	DOF = 105	-1.2
ECCENTRIC CRACK (ISIDA'S PROBLEM)	116 TRIANGULAR ELEMENTS PLUS 2 ESE, DOF = 152	-1.1 (SIDE A) +0.5 (SIDE B)	NONE	NONE

The computed stress-intensity factors for the two crack tips are

$$K_1 = 2.67496 \times 10^{-3} \text{ MPa} - \sqrt{m} \qquad K_2 = 0.25067 \times 10^{-3} \text{ MPa} - \sqrt{m}$$

These values include in their definition a factor of $\sqrt{\pi}$. To compare with the values in the Request for Proposal, it is necessary to divide by $\sqrt{\pi}$; hence,

$$K_1 = 1.50918 \times 10^{-3} \text{ MPa} - \sqrt{m} \qquad K_2 = 0.14143 \times 10^{-3} \text{ MPa} - \sqrt{m}$$

These values are quite close to those computed by Erdogan and Biricikoglu in ref. 19. The percentage of error is -0.12% and +0.75%, respectively. The axial stresses and displacements along the crack line are plotted in figures 17 and 18.

Stiffened Plate - The rate of growth of a crack in a stiffened plate will be influenced by the presence of the risers. The simple stiffened plate configuration shown in figure 19 has been analyzed to determine this effect. The plate is loaded by a stress along its edge normal to the crack. Two cracks are assumed to propagate from the center of the two edges of the plate toward the risers. When the cracks have passed underneath the risers, they are assumed to extend up the riser and into the plate at an equal rate until the riser is completely failed. The crack is then assumed to continue to propagate into the plate.

Only one quarter of the configuration shown in figure 19 is idealized, the remainder being represented by symmetric boundary restraints. Both the plate and the riser are idealized using triangular membrane elements. The 8-node crack element is used to represent the crack tip.

The results of the analysis is shown in figure 20 in the form of the crack tip symmetric stress-intensity factor plotted against the crack length. It is evident that the riser will have a considerable effect on the rate of crack growth.

Thermal Stress-Intensity Problem - Sih (ref. 21) has given the following plane-stress formulae for the stress-intensity factors appropriate to a crack with constant-temperature faces (see figure 21) acting as sinks for the steady, radially inward flow of heat Q at infinity.

$$K_1 = \frac{E \alpha Q(1 + \nu)\sqrt{a}}{4\sqrt{\pi}\,k} \qquad \text{and} \qquad K_{II} = O \tag{82}$$

In (82), α is the coefficient of thermal expansion, and k is the thermal conductivity. We now solve the associated temperature-distribution problem to obtain thermal input in a form acceptable to the computer program.

The general real solution for the temperature, T, in a steady heat-conduction problem in two dimensions is

44

$$T(x, y) = f(z) + \bar{f}(\bar{z}) \tag{83}$$

where f is an analytic function of $z = x + iy$. The symmetry of the problem indicated in figure 21 permits us to write

$$T(x, y) = T(x, -y) \tag{84}$$

which leads at once to

$$\bar{f}(\bar{z}) = f(\bar{z}) \tag{85}$$

permitting (83) to be written as

$$T(x, y) = f(z) + f(\bar{z}) \tag{86}$$

The constant-temperature condition for the crack faces requires that

$$\frac{\partial T}{\partial x} = f'(z) + f'(\bar{z}) \tag{87}$$

vanish on the crack faces; i.e.

$$f'^{+}(x) + f'^{-}(x) = 0 \quad , \quad x^2 < a^2 \tag{88}$$

In (87) and (88), prime (') denotes differentiation with respect to the parenthetical variable, while the superscript (+) or (−) indicates a value taken in the upper and lower half planes, respectively.

The boundary condition at infinity is

$$k \int_{0}^{2\pi} \frac{\partial T}{\partial r} \, r \, d\theta = Q \tag{89}$$

in which r and θ (shown in figure 21) are defined by

$$z = re^{i\theta} \tag{90}$$

In view of (89), $f'(z)$ is expected to vary at infinity like z^{-1}.

We now make the usual substitution for a cut-condition like (88); i.e.,

$$g(z) = \sqrt{z^2 - a^2} \; f'(z) \quad , \tag{91}$$

45

in which $\sqrt{z^2 - a^2}$ is that branch of $(z^2 - a^2)^{1/2}$ varying like z at infinity. Because of the anticipated remote behavior of $f'(z)$, we expect $g(z)$ to tend to a constant value at infinity.

The problem case in terms of $g(z)$ is then

$$g^+(x) - g^-(x) = 0 \quad , \quad x^2 < a^2 \quad ; \tag{92}$$

$$\lim_{z \to \infty} g(z) = c_1 \tag{93}$$

The obvious solution being

$$g(z) = c_1 \tag{94}$$

which leads to

$$f(z) = c_1 \ln(z + \sqrt{z^2 - a^2}) + c_2 \tag{95}$$

when (91) is integrated.

The constant c_2 in (95) only sets the temperature reference, which is thus far unspecified. Taking $c_2 = 0$ with no loss in general applicability, we find

$$\frac{\partial T}{\partial r} = \frac{2c_1}{r} \tag{96}$$

for large z. Upon imposing (89), we find

$$c_1 = \frac{Q}{4k\pi} \tag{97}$$

Thus, from (86), (95), and (97),

$$T(x, y) = \frac{Q}{4k\pi} \left[\ln(z + \sqrt{z^2 - a^2}) + \ln(\bar{z} + \sqrt{\bar{z}^2 - a^2}) \right] \tag{98}$$

and the constant crack-face temperature is given by

$$T_c = \frac{Q \ln a}{2k\pi} \tag{99}$$

Referring to figure 22, it is convenient to let

$$r_1 = \sqrt{(x+a)^2 + y^2} \qquad \theta_1 = \tan^{-1}\frac{y}{x+a}$$

$$r = \sqrt{x^2 + y^2} \qquad \theta = \tan^{-1}\frac{y}{x}$$

$$r_2 = \sqrt{(x-a)^2 + y^2} \qquad \theta_2 = \tan^{-1}\frac{y}{x-a}$$

then the temperature distribution can be written as

$$T(x,y) = \frac{Q}{4k\pi}\ln\left\{\left(r\cos\theta + \sqrt{r_1 r_2}\cos\frac{\theta_1 + \theta_2}{2}\right)^2 \right.$$

$$\left. + \left(r\sin\theta + \sqrt{r_1 r_2}\sin\frac{\theta_1 + \theta_2}{2}\right)^2\right\} \tag{100}$$

Figure 23 shows a finite-element representation of the first quadrant of the problem in figure 21. The eight-node symmetric cracked element ABCD represents the crack-tip neighborhood in the finite-element model. Input particulars are taken to be

$$\frac{Q}{k} = 255.928°K \quad \text{and} \quad a = 114.3 \text{ mm} \tag{101}$$

leading to a crack-face temperature from (99) of

$$T_c = 255.505°K \tag{102}$$

and triangular-element temperatures (centroidal) from (98).

The computer program was executed twice with additional material properties:

$$E = 68.95 \text{ GPa} \;, \quad \nu = 0.3 \quad \text{and} \quad \alpha = 1.8 \times 10^{-6} \text{ m.m}^{-1}.\text{K}^{-1} \tag{103}$$

In the first execution, the temperature of the cracked element was taken to correspond uniformly to that of the crack faces (102). The computed stress-intensity factor

$$K_I = 4.9137 \times 10^{-3} \text{ MPa} - \sqrt{m} \tag{104}$$

is 14.95% higher than the analytical value of 4.2747×10^{-3} MPa $-\sqrt{m}$. This is not unexpected in view of the fact that the entire cracked element is taking the crack-face temperature, a condition thermally more severe than the analytical temperature distribution (98). This is reflected in the results of the second execution, in which the temperature of the cracked element was taken to be 255.567°K, which corresponds to the average

47

of six superimposed triangles (shown dashed in figure 23). The stress-intensity factor computed for the second execution was

$$K_I = 3.6325 \times 10^{-3} \, MPa - \sqrt{m} \tag{105}$$

which is 15% lower than the analytical value. It is clear that more refinement in the crack-tip neighborhood would lead to a more tolerable discrepancy. It is important to point out that such refinement will not be necessary in more routine applications where the temperature gradients near the crack tip are less severe.

APPENDIX – ELEMENT STIFFNESS MATRICES

Axial Element

The positive sign convention for the axial element is illustrated in figure A-1. For this convention k and P_{rt} are as follows:

$$[k] = \frac{EA}{\ell} \begin{bmatrix} 1 & 1 \\ 1 & 1 \end{bmatrix}, \quad \{P_{rt}\} = -AE\alpha T \begin{Bmatrix} 1 \\ 1 \end{Bmatrix}$$

Triangular Membrane Element

The sign convention for the triangular membrane element is illustrated in figure A-2. Note that six displacements or degrees of freedom are present. It is then reasonable to assume the following displacement field.

$$u = a_1 + a_2 x + a_3 y \qquad v = a_4 + a_5 x + a_6 y$$

The displacements of the element can then be expressed in terms of the a_i coefficients as follows:

$$\begin{Bmatrix} u_1 \\ u_2 \\ u_3 \\ v_1 \\ v_2 \\ v_3 \end{Bmatrix} = \begin{bmatrix} 1 & & & & & \\ 1 & x_2 & & & & \\ 1 & x_3 & y_3 & & & \\ & & & 1 & & \\ & & & 1 & x_2 & \\ & & & 1 & x_3 & y_3 \end{bmatrix} \begin{Bmatrix} a_1 \\ a_2 \\ a_3 \\ a_4 \\ a_5 \\ a_6 \end{Bmatrix}$$

or in matrix notation

$$\{\delta\} = [C]\{a\}$$

then

$$\{a\} = [C]^{-1}\{\delta\}$$

49

where

$$[c]^{-1} = \frac{1}{x_2 y_3} \begin{bmatrix} x_2 y_3 & & & & & \\ -y_3 & y_3 & & & & \\ x_{32} & -x_3 & x_2 & & & \\ & & & x_2 y_3 & & \\ & & & -y_3 & y_3 & \\ & & & x_{32} & -x_3 & x_2 \end{bmatrix}$$

where $x_{32} = x_3 - x_2$.

The strains can also be expressed in terms of the displacement coefficients:

$$\epsilon_x = \frac{\partial u}{\partial x} = a_2 \qquad \epsilon_y = \frac{\partial v}{\partial y} = a_6$$

$$\gamma_{xy} = \frac{\partial u}{\partial y} + \frac{\partial v}{\partial x} = a_3 + a_5$$

Then

$$\begin{Bmatrix} \epsilon_x \\ \epsilon_y \\ \gamma_{xy} \end{Bmatrix} = \begin{bmatrix} 0 & 1 & 0 & 0 & 0 & 0 \\ 0 & 0 & 0 & 0 & 0 & 1 \\ 0 & 0 & 1 & 0 & 1 & 0 \end{bmatrix} \begin{Bmatrix} a_1 \\ a_2 \\ a_3 \\ a_4 \\ a_5 \\ a_6 \end{Bmatrix}$$

or

$$\{\epsilon\} = [B]\{a\}$$

If the strains and stresses are constant within the membrane element, the strain energy can be expressed as

$$S = \frac{1}{2} A_o t \{\sigma\}^T \{\epsilon\}$$

where A_o is the area of triangular element. Let the stress-strain relations for the anisotropic material in the elemental reference system be written as

50

$$\{\sigma\} = [A]\{\epsilon\}$$

Then the strain energy can be expressed in terms of the node point displacements as follows:

$$S = \frac{1}{2} A_0 t \{a\}^T [B]^T [A] [B] \{a\}$$

$$S = \frac{1}{2} A_0 t \{\delta\}^T [C^{-1}]^T [B]^T [A][B][C^{-1}] \{\delta\}$$

And the $[k]$ matrix for the triangular membrane element is, therefore,

$$[k] = A_0 t [C^{-1}]^T [B]^T [A] [B] [C^{-1}]$$

If the multiplication is carried out and if the elements of the matrix are arranged so that the convention in figure A-3 applies then the k_{ij} elements of the stiffness matrix are

$$\left(\frac{4A_0}{t}\right) k_{11} = y_3^2 A_{11} - 2y_3 x_{32} A_{13} + x_{32}^2 A_{33}$$

$$\left(\frac{4A_0}{t}\right) k_{12} = y_3^2 A_{13} - y_3 x_{32} (A_{12} + A_{33}) + x_{32}^2 A_{23}$$

$$\left(\frac{4A_0}{t}\right) k_{13} = -y_3^2 A_{11} + y_3 (x_3 + x_{32}) A_{13} - x_3 x_{32} A_{33}$$

$$\left(\frac{4A_0}{t}\right) k_{14} = -y_3^2 A_{13} + x_3 y_3 A_{12} + y_3 x_{32} A_{33} - x_3 x_{32} A_{23}$$

$$\left(\frac{4A_0}{t}\right) k_{15} = -x_2 y_3 A_{13} + x_2 x_{32} A_{33}$$

$$\left(\frac{4A_0}{t}\right) k_{16} = -x_2 y_3 A_{12} + x_2 x_{32} A_{23}$$

$$\left(\frac{4A_0}{t}\right) k_{22} = y_3^2 A_{33} - 2 y_3 x_{32} A_{23} + x_{32}^2 A_{22}$$

$$\left(\frac{4A_0}{t}\right) k_{23} = - y_3^2 A_{13} + x_3 y_3 A_{33} + y_3 x_{32} A_{12} - x_3 x_{32} A_{23}$$

51

$$\left(\frac{4A_o}{t}\right) k_{24} = -y_3^2 A_{33} + y_3 (x_3 + x_{32}) A_{23} - x_3 x_{32} A_{22}$$

$$\left(\frac{4A_o}{t}\right) k_{25} = x_2 x_{32} A_{23} - x_2 y_3 A_{33}$$

$$\left(\frac{4A_o}{t}\right) k_{26} = x_2 x_{32} A_{22} - x_2 y_3 A_{23}$$

$$\left(\frac{4A_o}{t}\right) k_{33} = y_3^2 A_{11} - 2x_3 y_3 A_{13} + x_3^2 A_{33}$$

$$\left(\frac{4A_o}{t}\right) k_{34} = y_3^2 A_{13} - x_3 y_3 (A_{12} + A_{33}) + x_3^2 A_{23}$$

$$\left(\frac{4A_o}{t}\right) k_{35} = x_2 y_3 A_{13} - x_2 x_3 A_{33}$$

$$\left(\frac{4A_o}{t}\right) k_{36} = x_2 y_3 A_{12} - x_2 x_3 A_{23}$$

$$\left(\frac{4A_o}{t}\right) k_{44} = y_3^2 A_{33} - 2x_3 y_3 A_{23} + x_3^2 A_{22}$$

$$\left(\frac{4A_o}{t}\right) k_{45} = -x_2 x_3 A_{23} + x_2 y_3 A_{33}$$

$$\left(\frac{4A_o}{t}\right) k_{46} = -x_2 x_3 A_{22} + x_2 y_3 A_{23}$$

$$\left(\frac{4A_o}{t}\right) k_{55} = x_2^2 A_{33}$$

$$\left(\frac{4A_o}{t}\right) k_{56} = x_2^2 A_{23}$$

$$\left(\frac{4A_o}{t}\right) k_{66} = x_2^2 A_{22}$$

where $A_o = \frac{1}{2} x_2 y_3$

$$x_{32} = x_3 - x_2$$

The values of P_{rt} for the triangular plate element can be computed in terms of the element stiffness matrix. Note that

$$\{P\} = [k]\{p\} + \{P_{rt}\}$$

If $\{P\} = 0$ and $\{p\}$ is selected as the thermal displacement for free expansion, then the forces for complete restraint are

$$\{P_{rt}\} = -[k]\{p_o\}$$

For the triangular plate element, the components of $\{p_o\}$ are

$$u_1 = 0$$

$$u_2 = \alpha^*_{11} T x_2$$

$$u_3 = \alpha^*_{11} T x_3 + \alpha^*_{12} T y_3$$

$$v_1 = 0$$

$$v_2 = 0$$

$$v_3 = \alpha^*_{22} T y_3$$

The symbol * implies that the thermal expansion coefficients have been rotated into the local reference axis for the element.

Spring or Fastener Element

Figure A-4 illustrates two plates connected by a shear pin, and the direction vectors for the system of forces that are assumed to act on the pin are illustrated in figure A-5. For the spring element, it is necessary to define four node points. Node points (1) and (2) define the element itself. In most structural models these node points may be coincident before any strains occur, that is, $(Z_1 - Z_2) = 0$. Node points (3) and (4) are used in conjunction with node point (1) to define direction vectors for spring elements K_1 and K_2, respectively. K_3 is assumed to be a spring element perpendicular to the plane containing K_1 and K_2. In other words, the system of spring elements is that illustrated in figure A-6. If we let u, v, w, be displacements, the element forces for the spring system are

53

$$P_{x1} = K_1 (u_1 - u_2)$$

$$P_{y1} = K_2 (v_1 - v_2)$$

$$P_{z1} = K_3 (w_1 - w_2)$$

$$P_{x2} = -P_{x1}$$

$$P_{y2} = -P_{y1}$$

$$P_{z2} = -P_{z1}$$

Hence, the stiffness matrix is

$$
[k] =
\begin{bmatrix}
K_1 & 0 & 0 & -K_1 & 0 & 0 \\
0 & K_2 & 0 & 0 & -K_2 & 0 \\
0 & 0 & K_3 & 0 & 0 & -K_3 \\
-K_1 & 0 & 0 & K_1 & 0 & 0 \\
0 & -K_2 & 0 & 0 & K_2 & 0 \\
0 & 0 & -K_3 & 0 & 0 & K_3
\end{bmatrix}
$$

where K_1, K_2, and K_3 are linear spring stiffnesses for the fastener element.

10-Node Cracked Element Thermal Effects

Let the coordinate system for the ten node cracked element be the one illustrated in figure A-7. The stress-strain law can be written as

$$
\begin{Bmatrix} \epsilon_x \\ \epsilon_y \\ \gamma_{xy} \end{Bmatrix}
=
\begin{bmatrix}
a_{11} & a_{12} & a_{16} \\
a_{12} & a_{22} & a_{26} \\
a_{16} & a_{26} & a_{66}
\end{bmatrix}
\begin{Bmatrix} \sigma_x \\ \sigma_y \\ \tau_{xy} \end{Bmatrix}
+
\begin{Bmatrix} \alpha_{11}T \\ \alpha_{22}T \\ \alpha_{12}T \end{Bmatrix}
$$

54

Assume a constant temperature distribution over the element; then, for free expansion

$$\{\sigma\} = \{0\}$$

and

$$\epsilon_x = \frac{\partial u}{\partial x} = \alpha_{11}T$$

$$\epsilon_y = \frac{\partial v}{\partial y} = \alpha_{22}T$$

$$\gamma_{xy} = \frac{\partial u}{\partial y} + \frac{\partial v}{\partial x} = \alpha_{12}T$$

The displacement function is then of the form

$$u = \alpha_{11}Tx + C_2\alpha_{12}Ty + C_1$$

$$v = \alpha_{22}Ty + C_4\alpha_{12}Tx + C_3$$

If $u_1 = v_1 = v_6 = 0$, the displacement functions become

$$u = \alpha_{11}Tx + \alpha_{12}Ty$$

$$v = \alpha_{22}Ty$$

As in the case of the triangular plate element

$$\{P_{rt}\} = -\left[k\right]\{P_o\}$$

where the element of p_o are

$$u_1 = 0 \qquad\qquad v_3 = -\alpha_{22}T\Delta$$

$$v_1 = 0 \qquad\qquad u_4 = -\alpha_{12}T\Delta$$

$$u_2 = -\alpha_{11}T\Delta \qquad\qquad v_4 = -\alpha_{22}T\Delta$$

$$v_2 = 0 \qquad\qquad u_5 = \alpha_{11}T\Delta - \alpha_{12}T\Delta$$

$$u_3 = -\alpha_{11}T\Delta - \alpha_{12}T\Delta \qquad\qquad v_5 = -\alpha_{22}T\Delta$$

55

$$u_6 = \alpha_{11} T \Delta \qquad\qquad v_8 = \alpha_{22} T \Delta$$

$$v_6 = 0 \qquad\qquad u_9 = -\alpha_{11} T \Delta + \alpha_{12} T \Delta$$

$$u_7 = \alpha_{11} T \Delta + \alpha_{12} T \Delta \qquad\qquad v_9 = \alpha_{22} T \Delta$$

$$v_7 = \alpha_{22} T \Delta \qquad\qquad u_{10} = -\alpha_{11} T \Delta$$

$$u_8 = \alpha_{12} T \Delta \qquad\qquad v_{10} = 0$$

REFERENCES

1. Kobayashi, A. S., et al.: Application of the Method of Finite Element Analysis to Two-Dimensional Problems in Fracture Mechanics. ONR Contract Nonr-477(39), NR 064 478, TR No. 5, University of Washington, Department of Mechanical Engineering, October 1968.

2. Chan, S. K.; Tuba, I. S.; and Wilson, W. K.: On the Finite Element Method in Linear Fracture Mechanics. J. of Eng. Fracture Mechanics, Vol. 2, No. 1, July 1970, pp. 1-17.

3. Oglesby, J. J.; and Lomacky, O.: An Evaluation of Finite Element Methods for the Computation of Elastic Stress Intensity Factors. Navy Ship Research and Development Center, NAVSHIPS Project SF 35.422.210, Task 15055, Report No. 3751, December 1971.

4. Byskov, E.: The Calculation of Stress Intensity Factors Using the Finite Element Method with Cracked Elements. International Journal of Fracture Mechanics, Vol. 6, No. 2, June 1970, pp. 159-167.

5. Tracey, D. M.: Finite Elements for Determination of Crack Tip Elastic Stress Intensity Factors. Engineering Fracture Mechanics, Vol. 3, 1971, pp. 255-265.

6. Walsh, P. F.: The Computation of Stress Intensity Factors by a Special Finite Element Technique. Internal Journal of Solids and Structures, Vol. 7, 1971, pp. 1333-1342.

7. Creager, M.: Development of a Cracked Finite Element. Lockheed-California Company Report, LR23996, December 1970.

8. Pian, T. H. H., et al.: Elastic Crack Analysis by a Finite Element Hybrid Method. Massachusetts Institute of Technology, Air Force Office of Scientific Research Contract F44620-67-C-0019.

9. Wilson, W. K.: Crack Tip Finite Elements for Plane Elasticity. Westinghouse Research Laboratories Scientific Paper 71-1E7, FMPWR-P2, June 7, 1971.

10. Aberson, J. A.: Cracked Finite Element Development at Lockheed-Georgia Company. LG73ER0007, Lockheed-Georgia Company, September 17, 1973.

11. Tsai, S. W.; and Hahn, H. T.: Recent Developments in Fracture of Filamentary Composites. Proceedings of an International Conference on Prospects of Fracture Mechanics, June 24-28, 1974, pp. 493-508.

12. Martin, H. C.: Introduction to Matrix Methods of Structural Analysis. McGraw-Hill Book Company, Inc., New York, 1966.

13. Przemieniecki, J. S.: Theory of Matrix Structural Analysis. McGraw-Hill Book Company, Inc., New York, 1968.

14. Williams, M. L.: Stress Singularities Resulting from Various Boundary Conditions in Angular Corners of Plates in Extension. J. of Applied Mechanics, Vol. 19, December 1952, pp. 526-528.

15. Williams, M. L.: On the Stress Distribution at the Base of a Stationary Crack. J. of Applied Mechanics, Vol. 24, No. 1, March 1957, pp. 109-114.

16. Paris, P. C.; and Sih, G. C.: Stress Analysis of Cracks. Fracture Toughness Testing and Its Application, ASTM STP 381, pp. 60.

17. Snyder, M. D.; and Cruse, T. A.: Crack Tip Stress Intensity Factors in Finite Anisotropic Plates. Air Force Materials Laboratory, AFML-TR-73-209, August 1973.

18. Sih, G. C.; Paris, P. C.; and Irwin, G. R.: On Cracks in Rectilinearly Anisotropic Bodies. International J. of Fracture Mechanics, Vol. 1, No. 3, 1965, pp. 189-202.

19. Erdogan, F.; and Biricikoglu, V.: Two Bonded Half Planes with a Crack Going Through the Interface. International J. of Engineering Science, Vol. 2, No. 7, July 1973.

20. Wilhem, D. P.: Fracture Mechanics Guidelines for Aircraft Structural Applications. Air Force Flight Dynamics Laboratory, AFFDL-TR-69-111, February 1970.

21. Sih, G. C.: On the Singular Character of Thermal Stresses Near a Crack Tip. Journal of Applied Mechanics, Vol. 29, No. 3, September 1962, pp. 587-589.
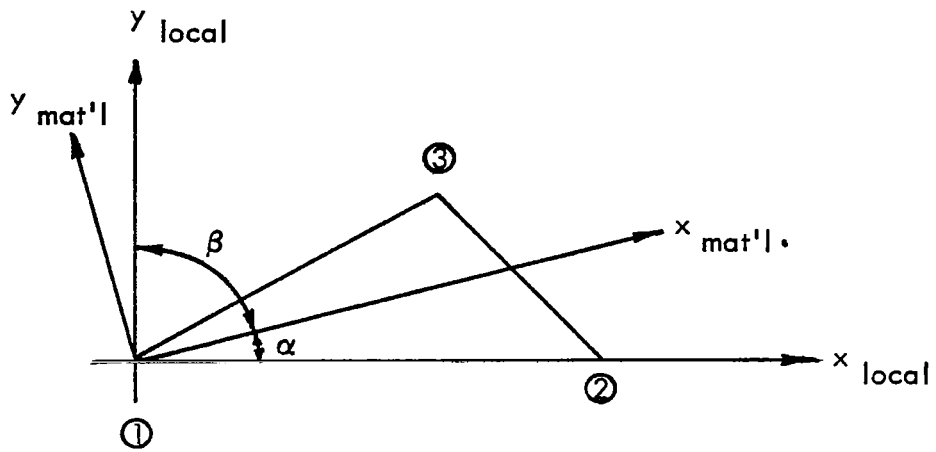
FIGURE 1.   TRIANGULAR ELEMENT MATERIAL AXIS
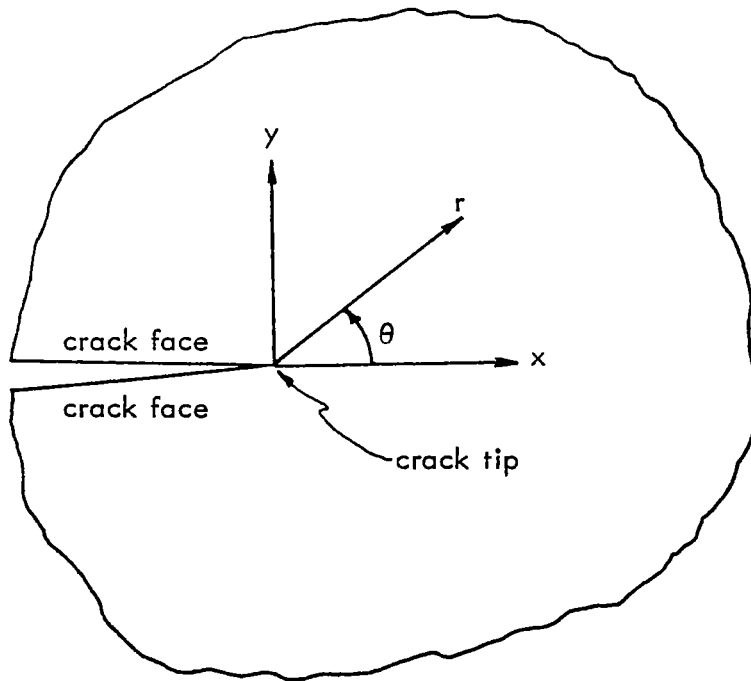
FIGURE 2.   CRACK-TIP NEIGHBORHOOD

59
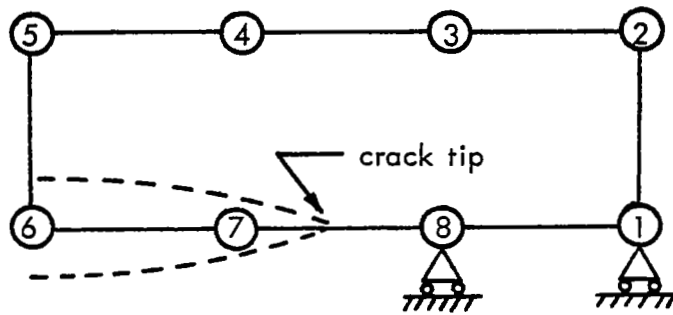
(a) 8-node Symmetric Cracked Element
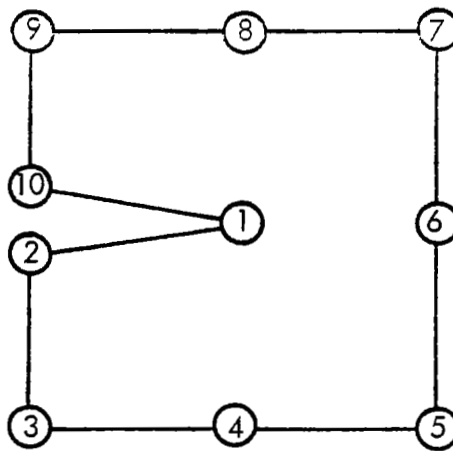
(b) 10-node Unsymmetric Cracked Element

FIGURE 3. CRACKED FINITE ELEMENTS
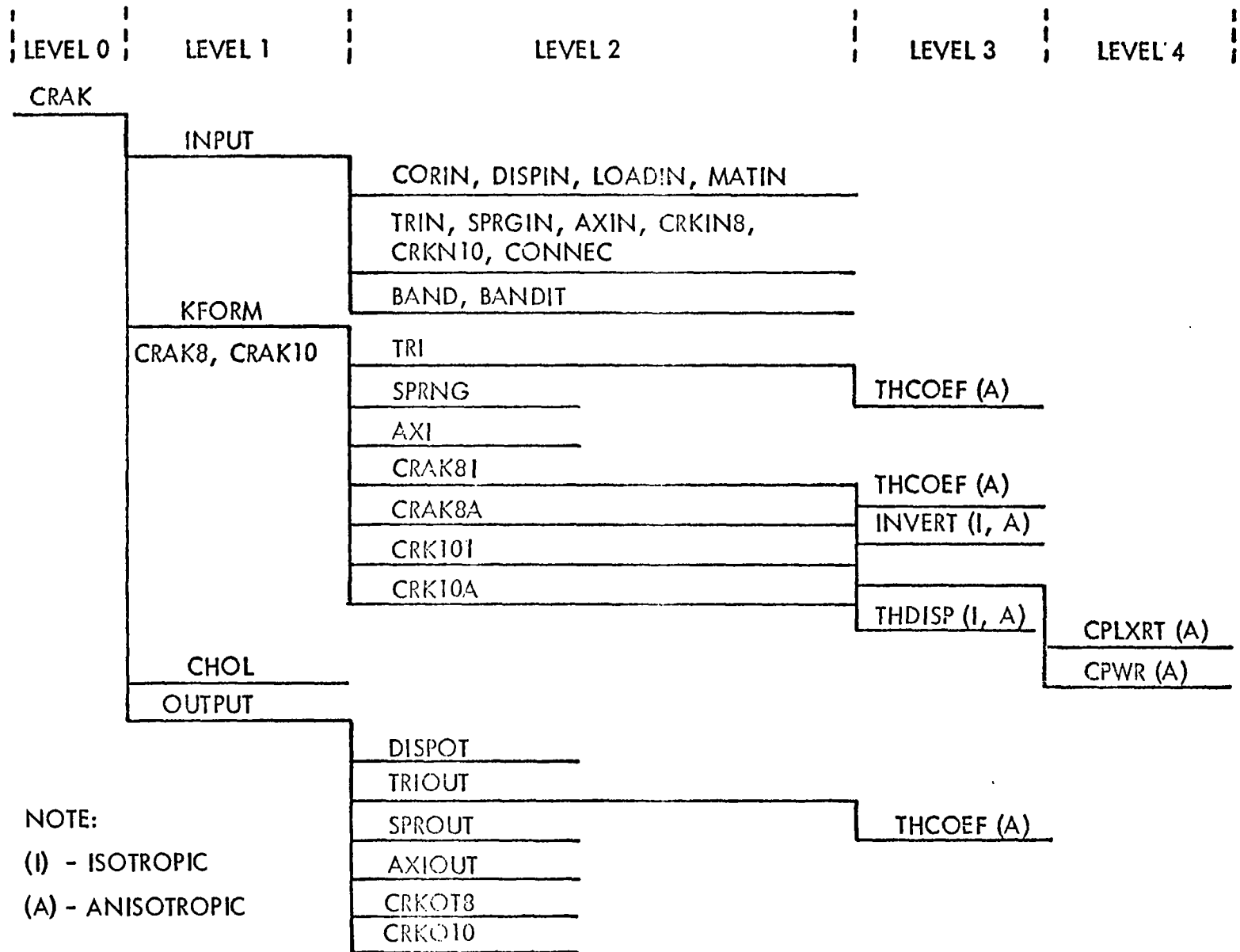
FIGURE 4. SEGMENT STRUCTURE FOR COMPUTER PROGRAM

NOTE:

(I) – ISOTROPIC

(A) – ANISOTROPIC
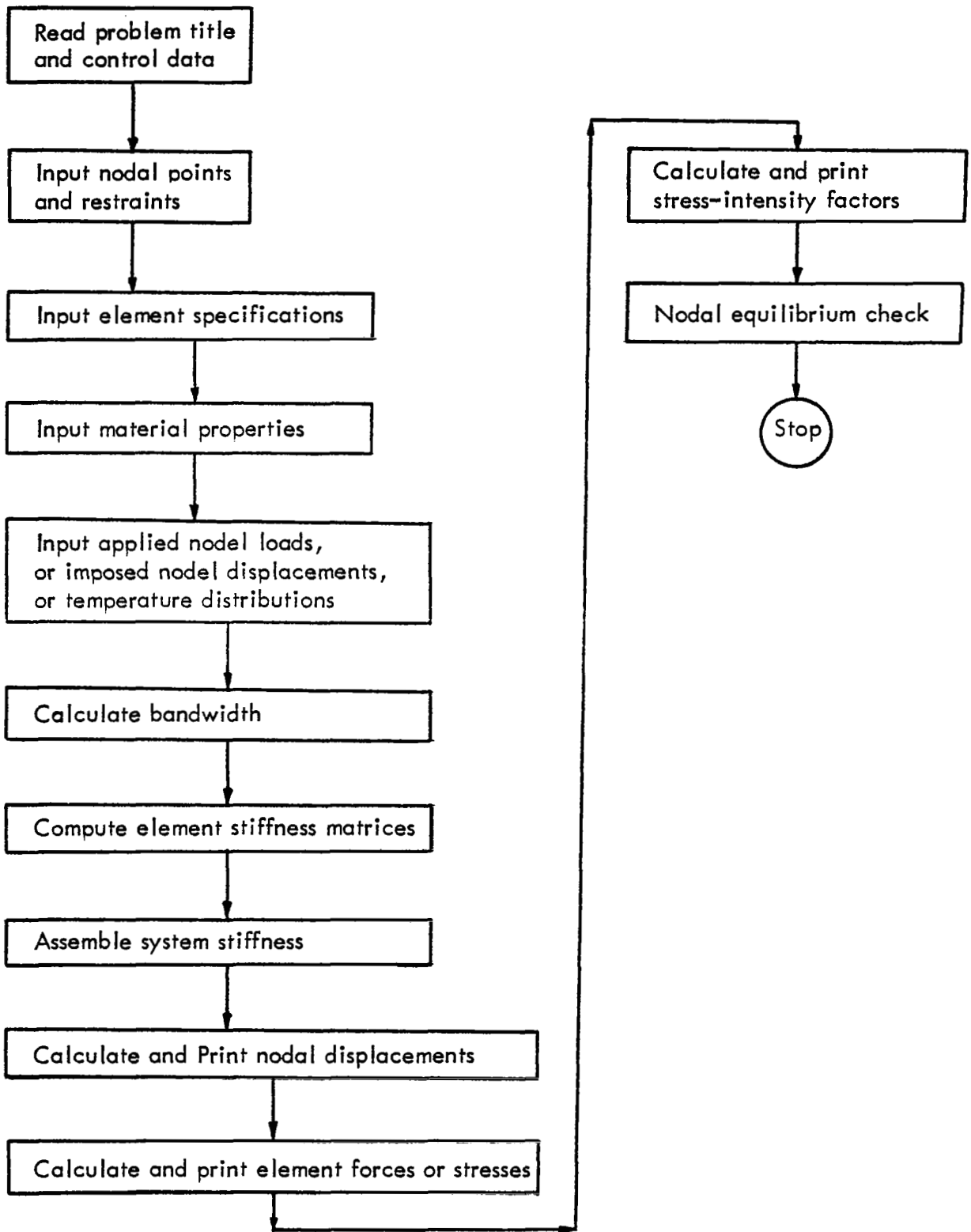
FIGURE 5.   OVERALL LOGIC FLOW OF COMPUTER PROGRAM

CENTER CRACK

DOUBLE-EDGE CRACK

30.48
(or 45.72 mm)

228.6 mm

15.24 mm

15.24 mm

76.2 mm

76.2 mm
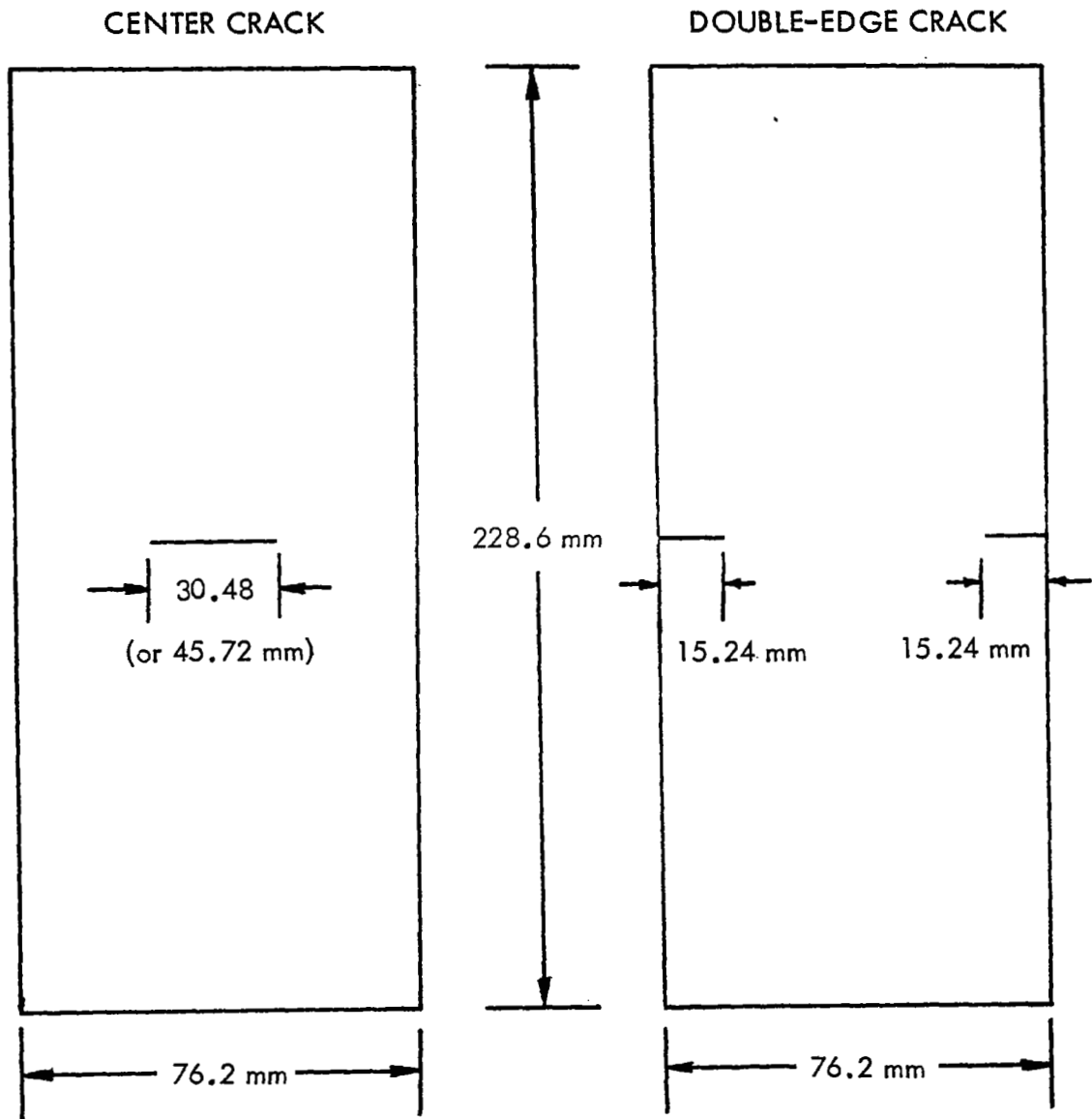
FIGURE 6.   CENTER-CRACKED AND DOUBLE-EDGE-CRACKED
ORTHOTROPIC TENSION PLATE

63

8-NODE SYMMETRIC
CRACKED ELEMENT

10-NODE UNSYMMETRIC
CRACKED ELEMENT

CRACKED
ELEMENT

CRACKED
ELEMENT
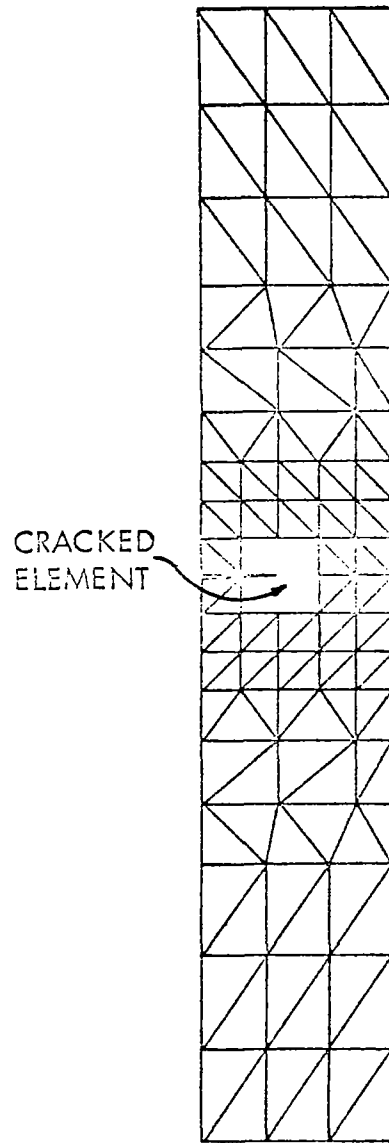
CRACK

FIGURE 7.   CRACKED ORTHOTROPIC TENSION PLATE
FINITE-ELEMENT MODELS
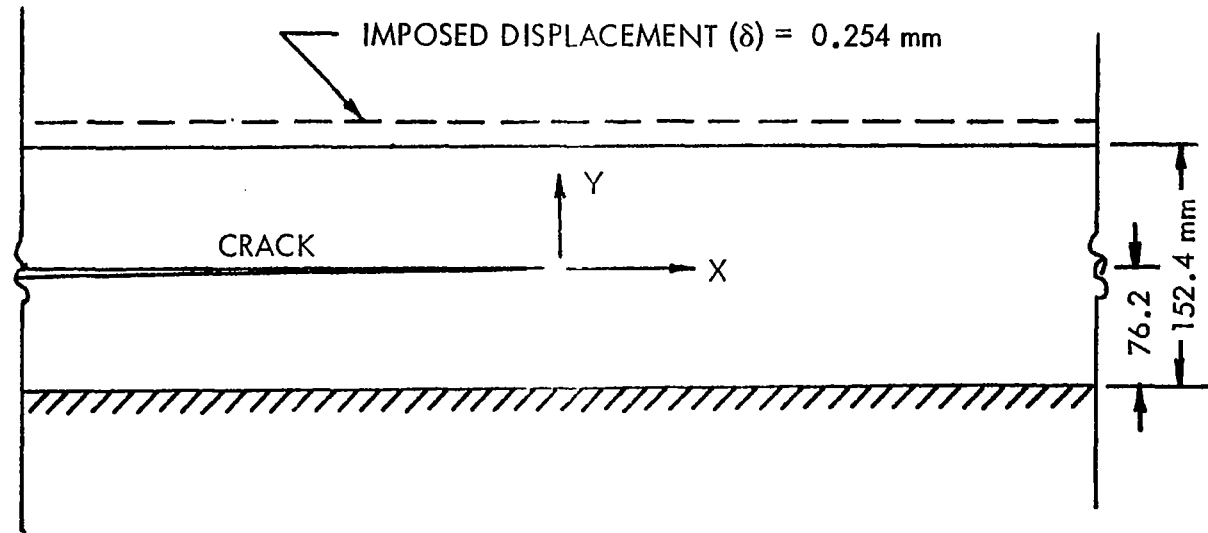
FIGURE 8. A LONGITUDINALLY CRACKED ORTHOTROPIC STRIP

CRACKED
ELEMENT
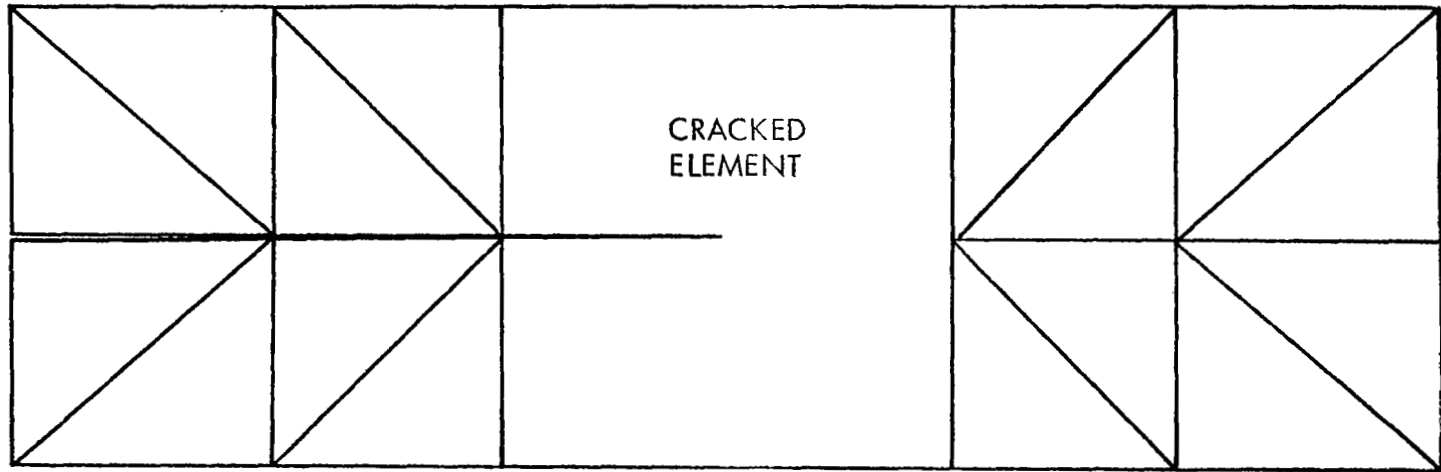
CRUDE MODEL
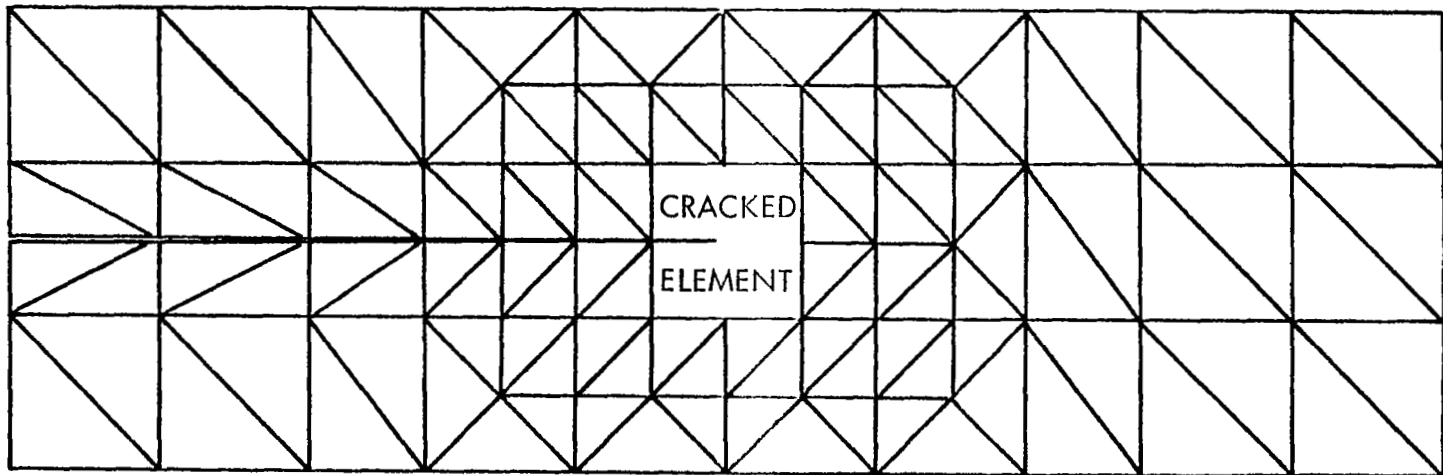
CRACKED

ELEMENT

DETAIL MODEL

FIGURE 9. FINITE-ELEMENT MODELS FOR A LONGITUDINALLY CRACKED ORTHOTROPIC STRIP
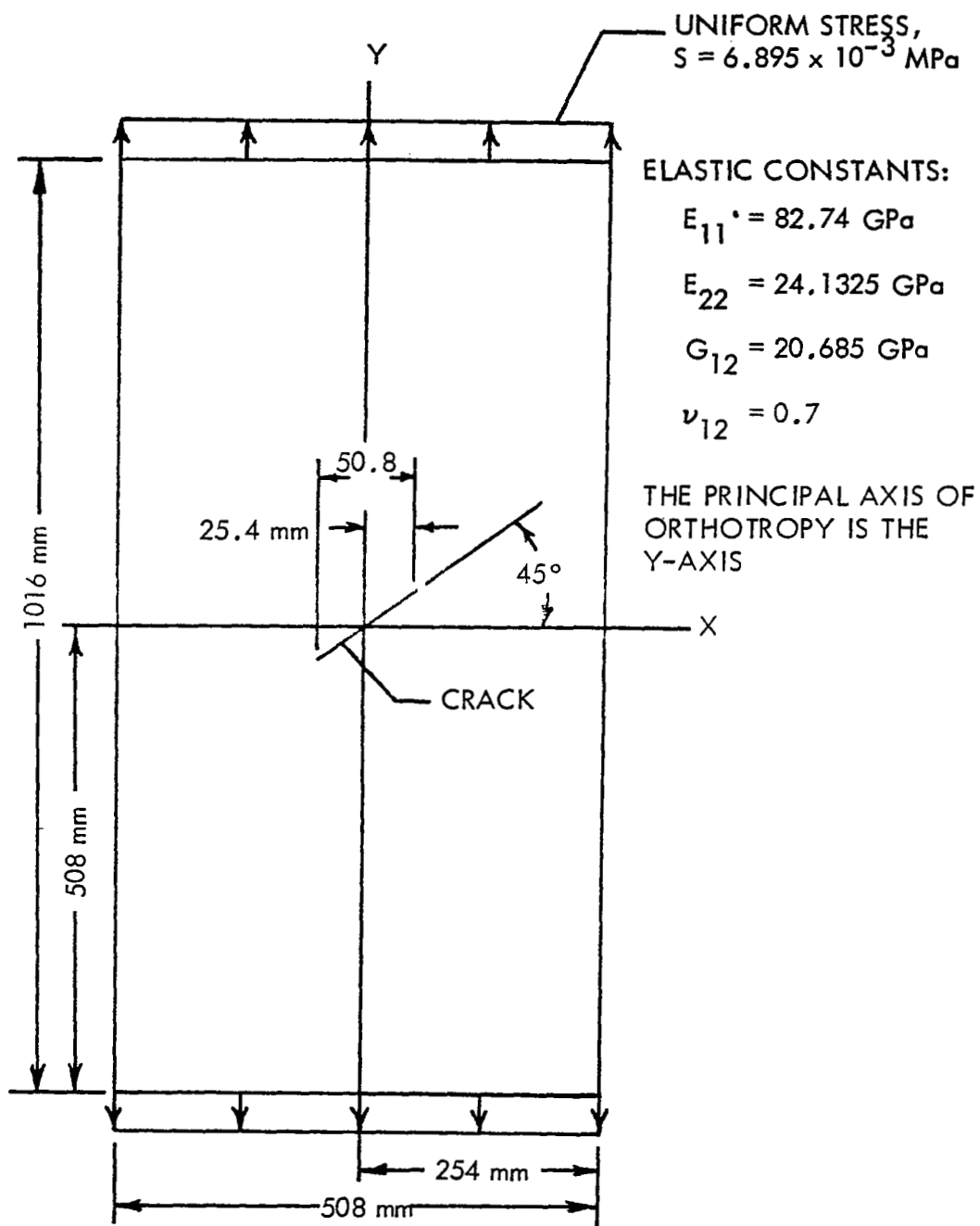
FIGURE 10.   45° CRACKED FINITE ORTHOTROPIC PLATE
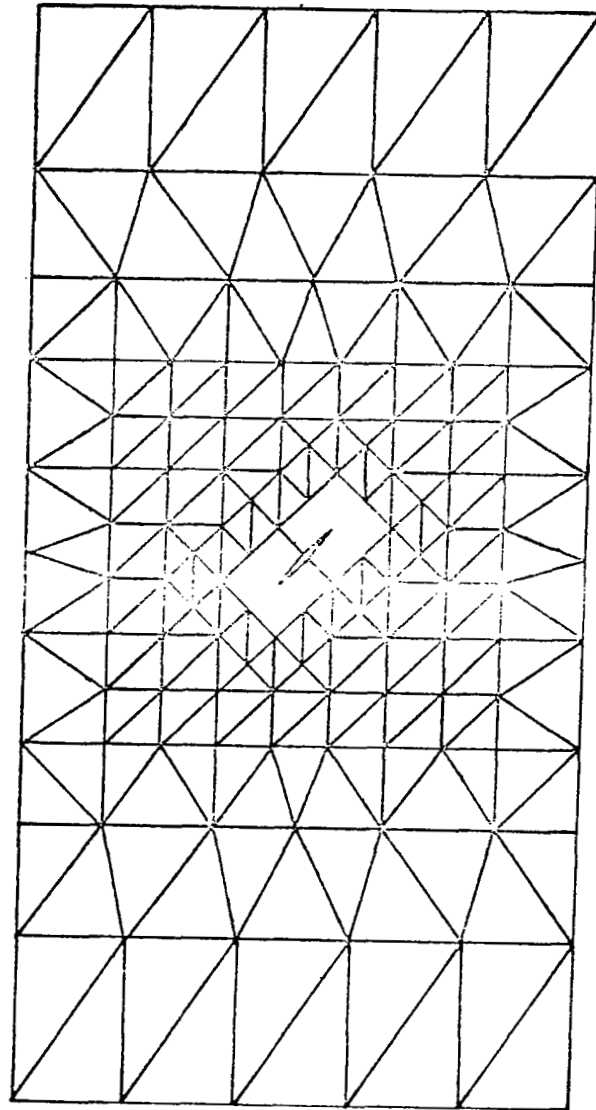
FIGURE 11. 45° CRACKED ORTHOTROPIC PLATE
FINITE-ELEMENT MODEL

68

FINITE ELEMENT MODEL

K_I % ERROR = -1.2

FINITE ELEMENT MODEL

K_I % ERROR = -1.5

FINITE ELEMENT MODEL

K_I % ERROR = +0.15

FINITE ELEMENT MODEL = 57 DOF, 35 CONSTANT-STRAIN TRIANGLE

8-NODE SYMMETRIC ELEMENT
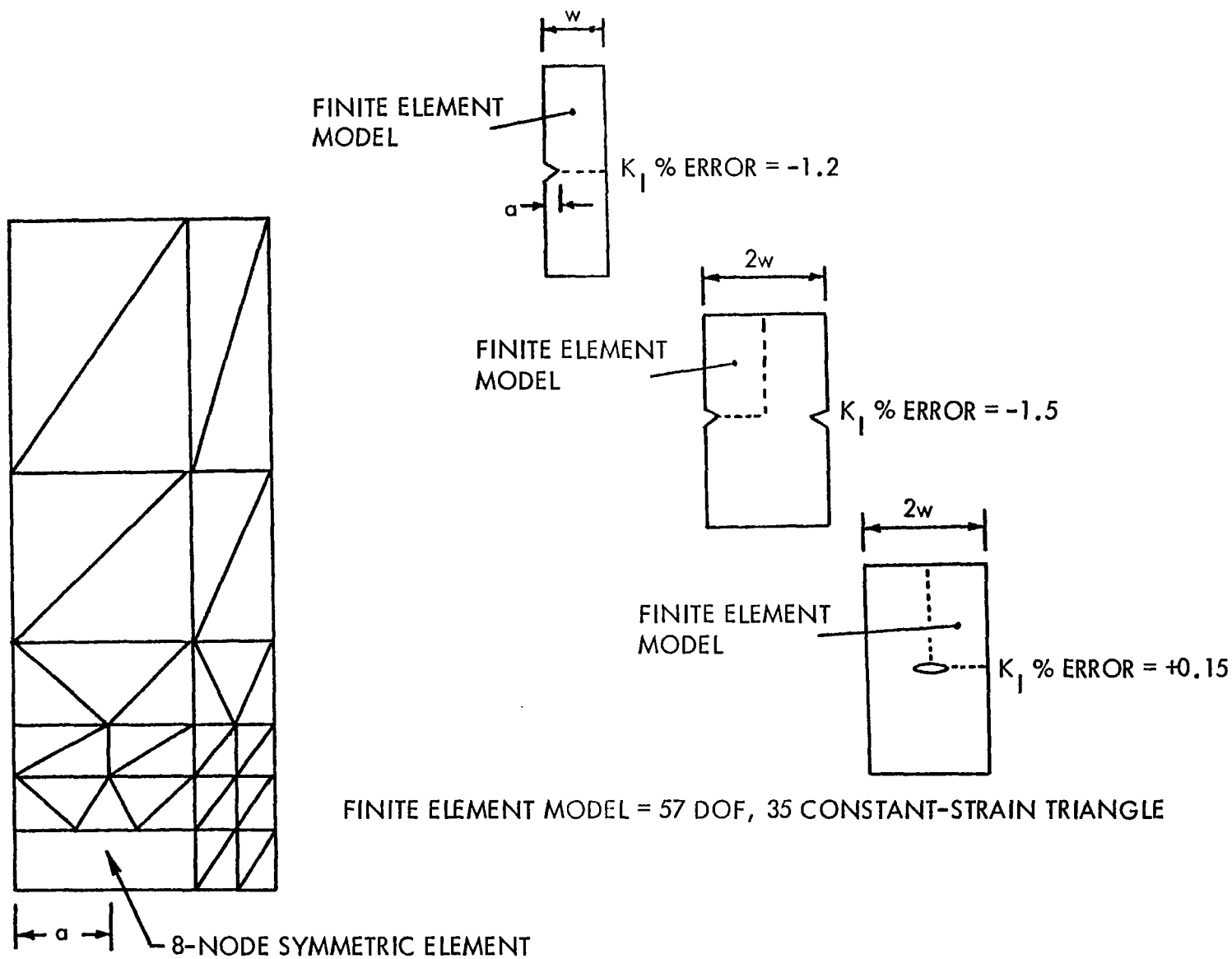
FIGURE 12. SYMMETRIC CRACKED ELEMENT MODEL FOR
SINGLE-EDGE, DOUBLE-EDGE, AND CENTER
CRACKED TENSION PANELS ($a/w = 1/3$)

K$_I$ % ERROR = -2.6%

K$_I$ % ERROR = -2.6%

K$_I$ % ERROR = -1.2%

10-NODE
UNSYMMETRIC
ELEMENT
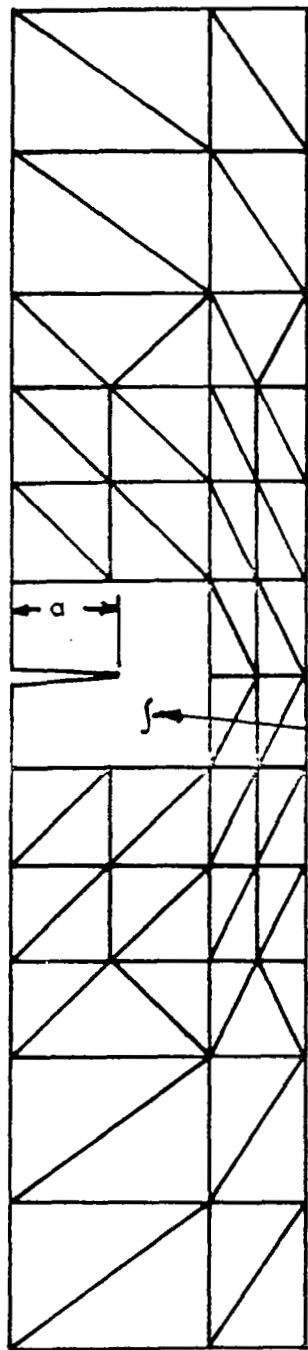
DOF = 105
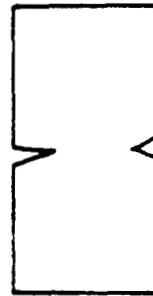
ELEMENTS = 69

FIGURE 13.   UNSYMMETRIC CRACKED ELEMENT MODEL FOR
SINGLE-EDGE, DOUBLE-EDGE, AND CENTER
CRACKED TENSION PANELS ($a/w = 1/3$)

K_I % ERROR = -1.1

K_I % ERROR = +0.5

A B

DOF = 152   ELEMENTS = 113
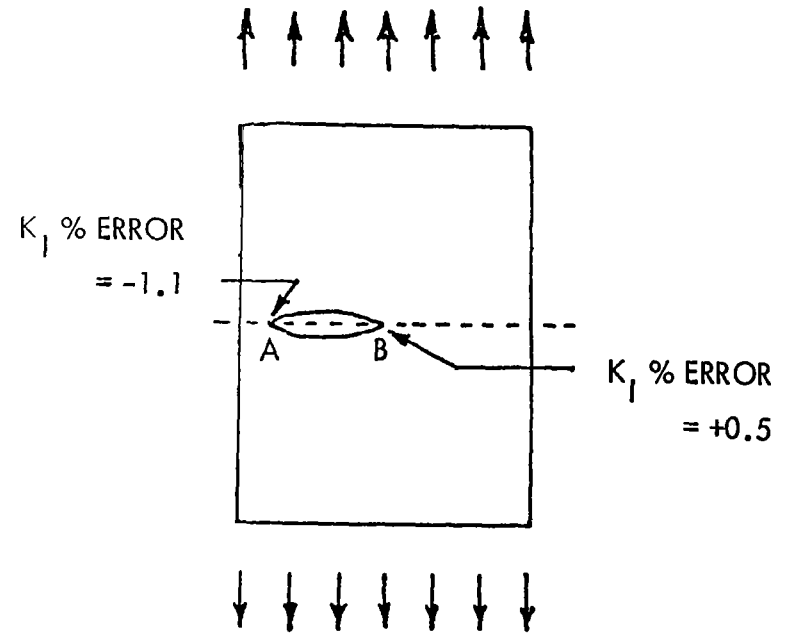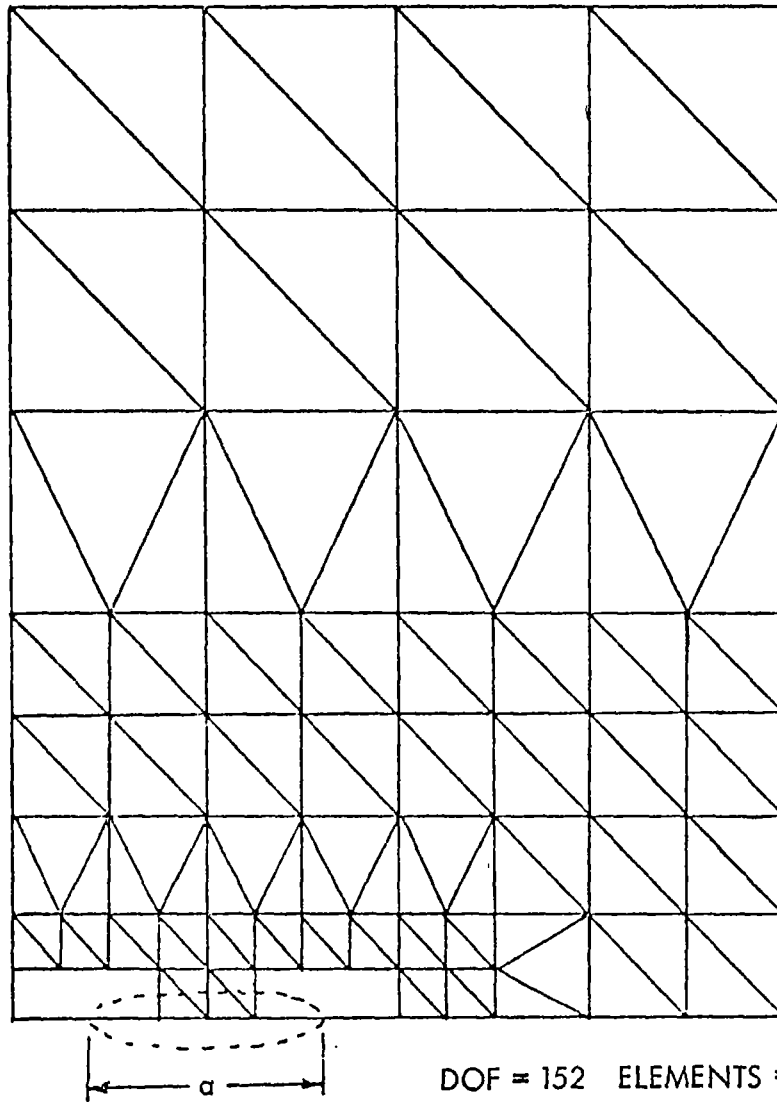
FIGURE 14.   ECCENTRIC CRACK (ISIDA'S PROBLEM) MODEL WITH TWO 8-NODE CRACKED ELEMENTS

UNIFORM DISPLACEMENT, EQ. (81)

MATERIAL 1   MATERIAL 2

1016 mm

508 mm

50.8 mm

44.45 mm

X

CRACK

254 mm

508 mm

YOUNG'S MODULUS

$E_1 = 68.950$ GPa

$E_2 = 30.683$ GPa

POISSON'S RATIO,

$\nu_1 = 0.30$

$\nu_2 = 0.35$

STRESS INTENSITY FACTOR
(REFERENCE 19)

$K_1 = 1.375 S_1$

$K_2 = 2.768 S_2$

WHERE S IS REMOTE STRESS.
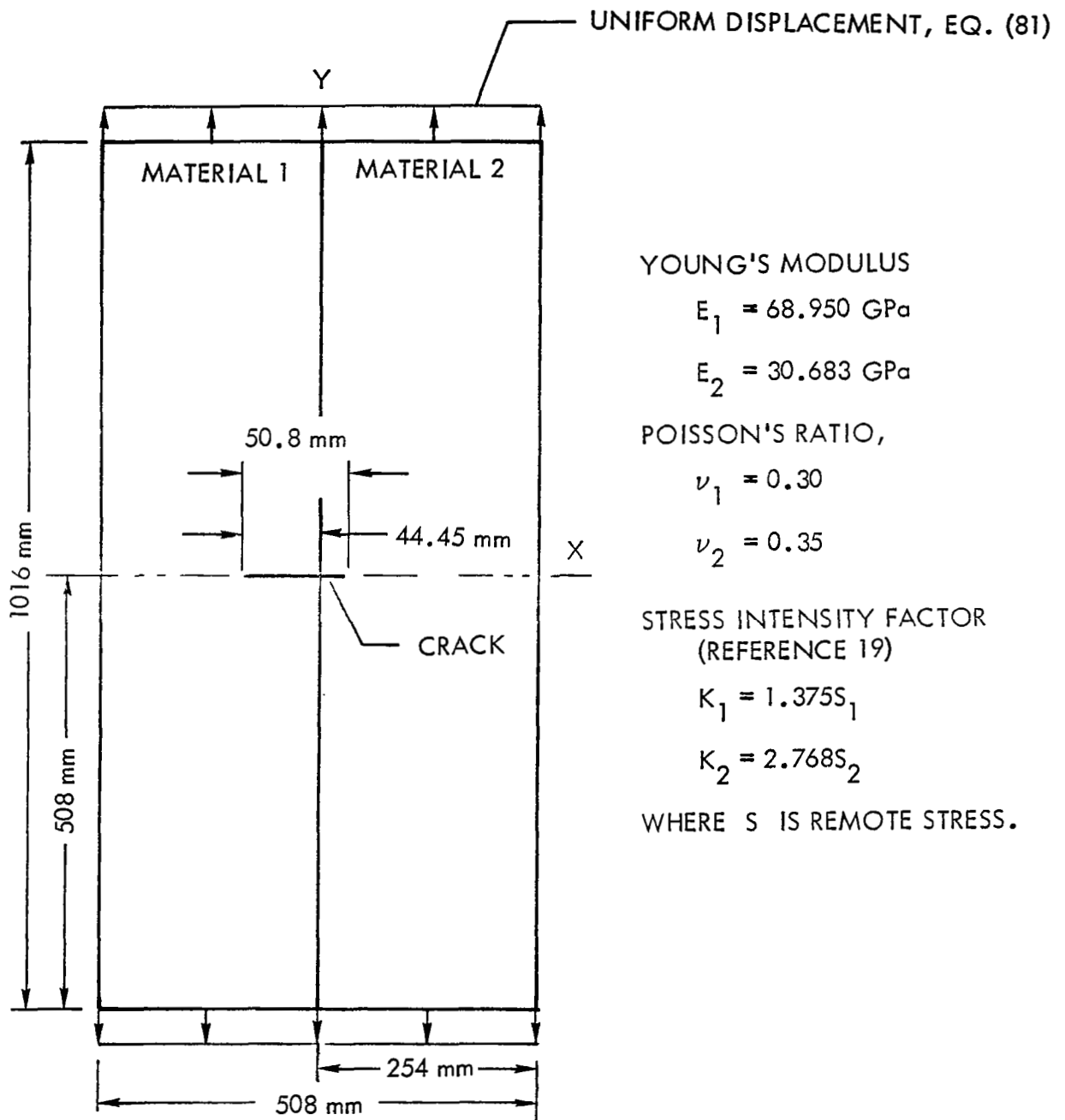
FIGURE 15.   BI-MATERIAL CRACKED PLATE
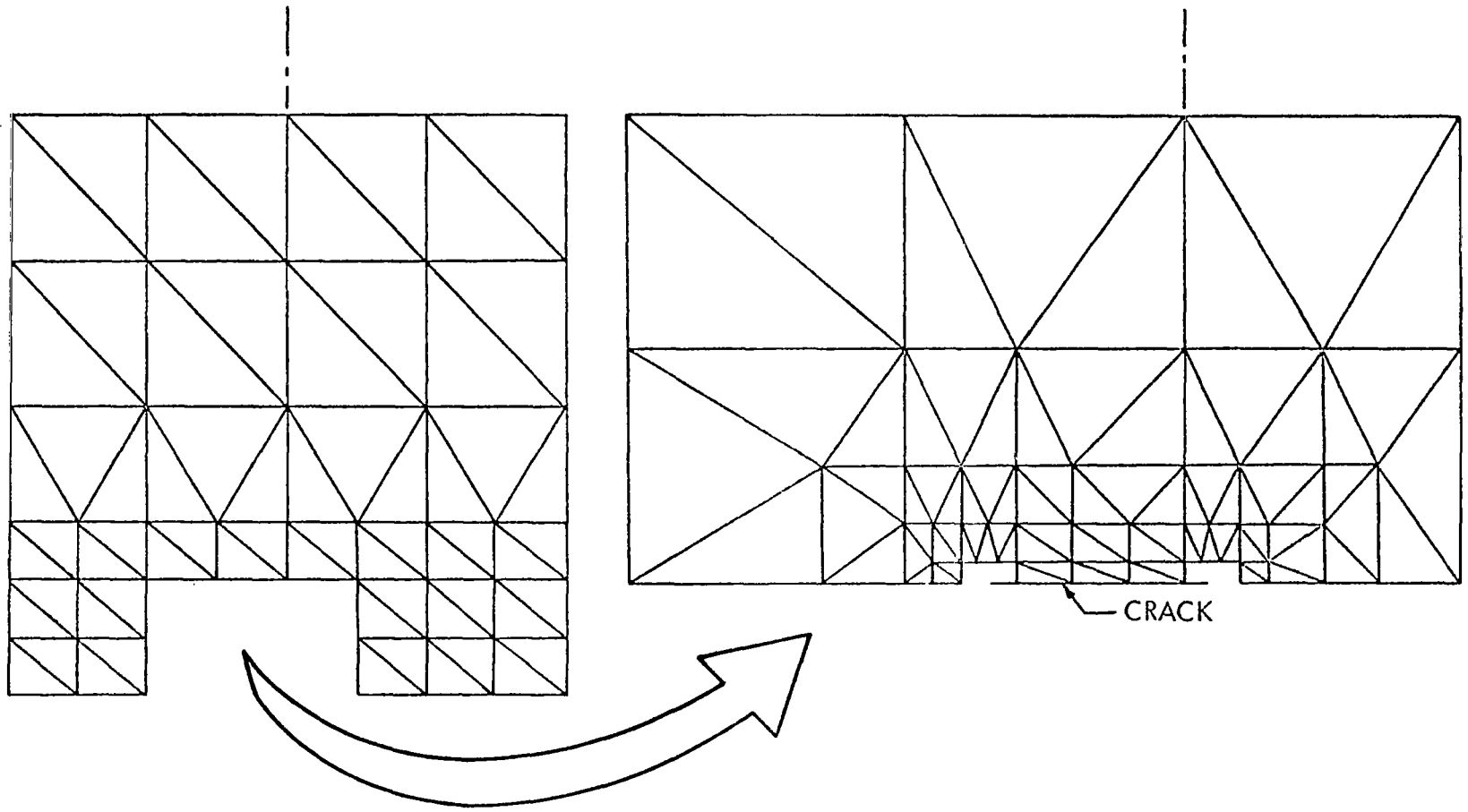
FIGURE 16.   BI-MATERIAL PLATE FINITE-ELEMENT MODEL
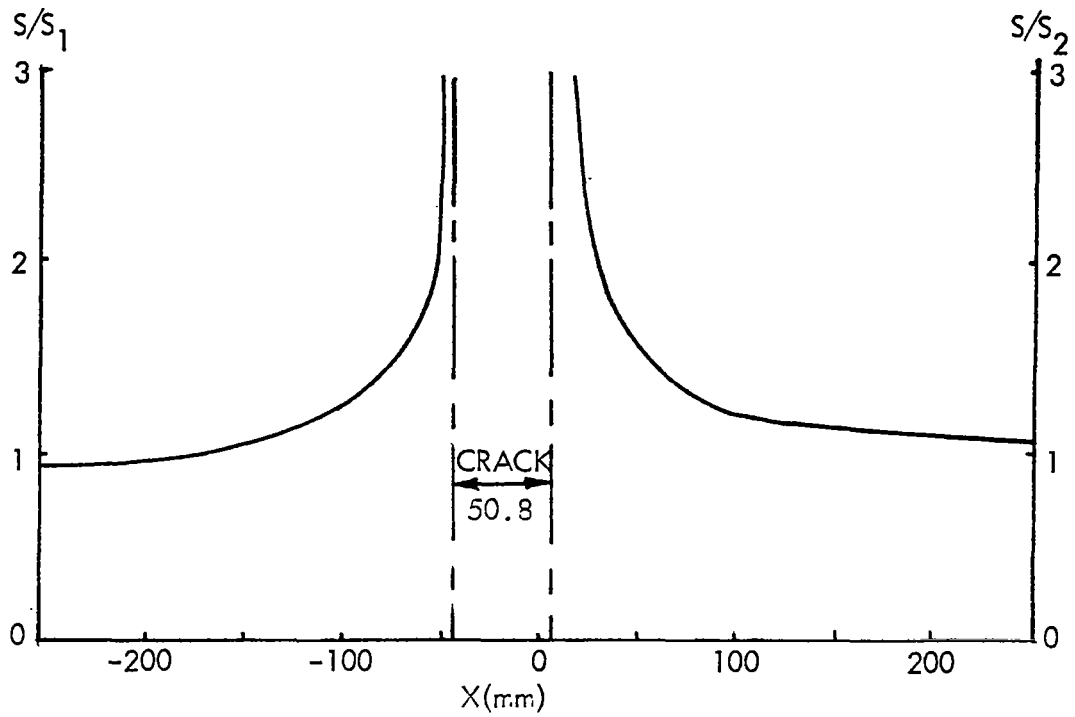
CRACK

FIGURE 17.   STRESS IN BI-MATERIAL CRACKED PLATE
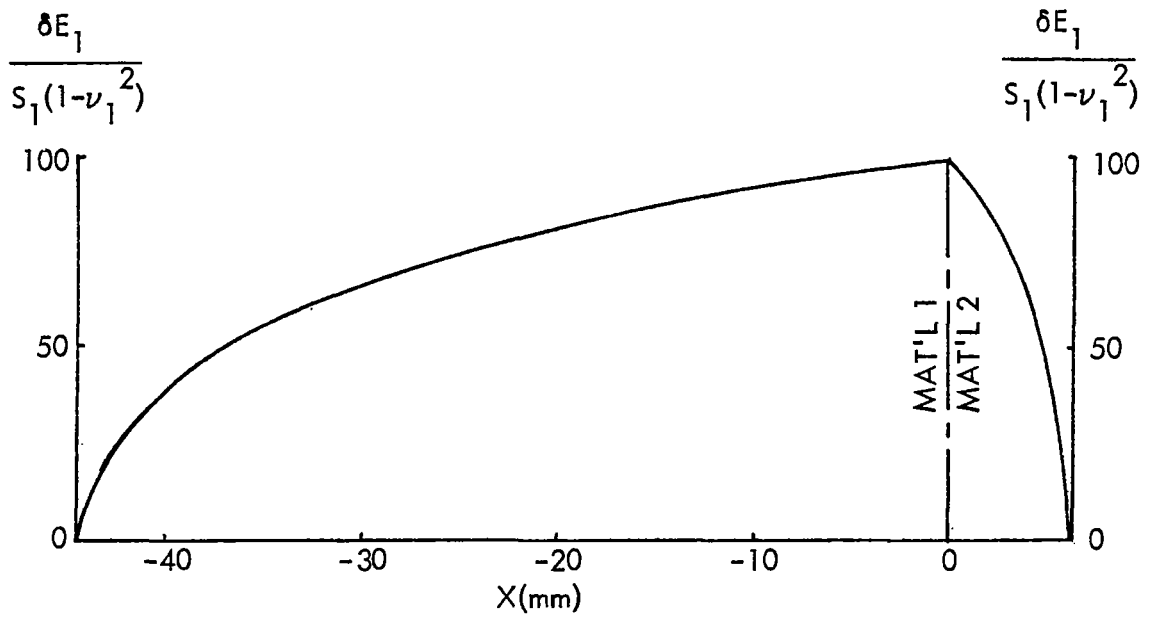
FIGURE 18.   DISPLACEMENTS OF CRACKED FACES
IN BI-MATERIAL PLATE

74

484 TRIANGULAR ELEMENTS
NUMBER OF DOF: 370
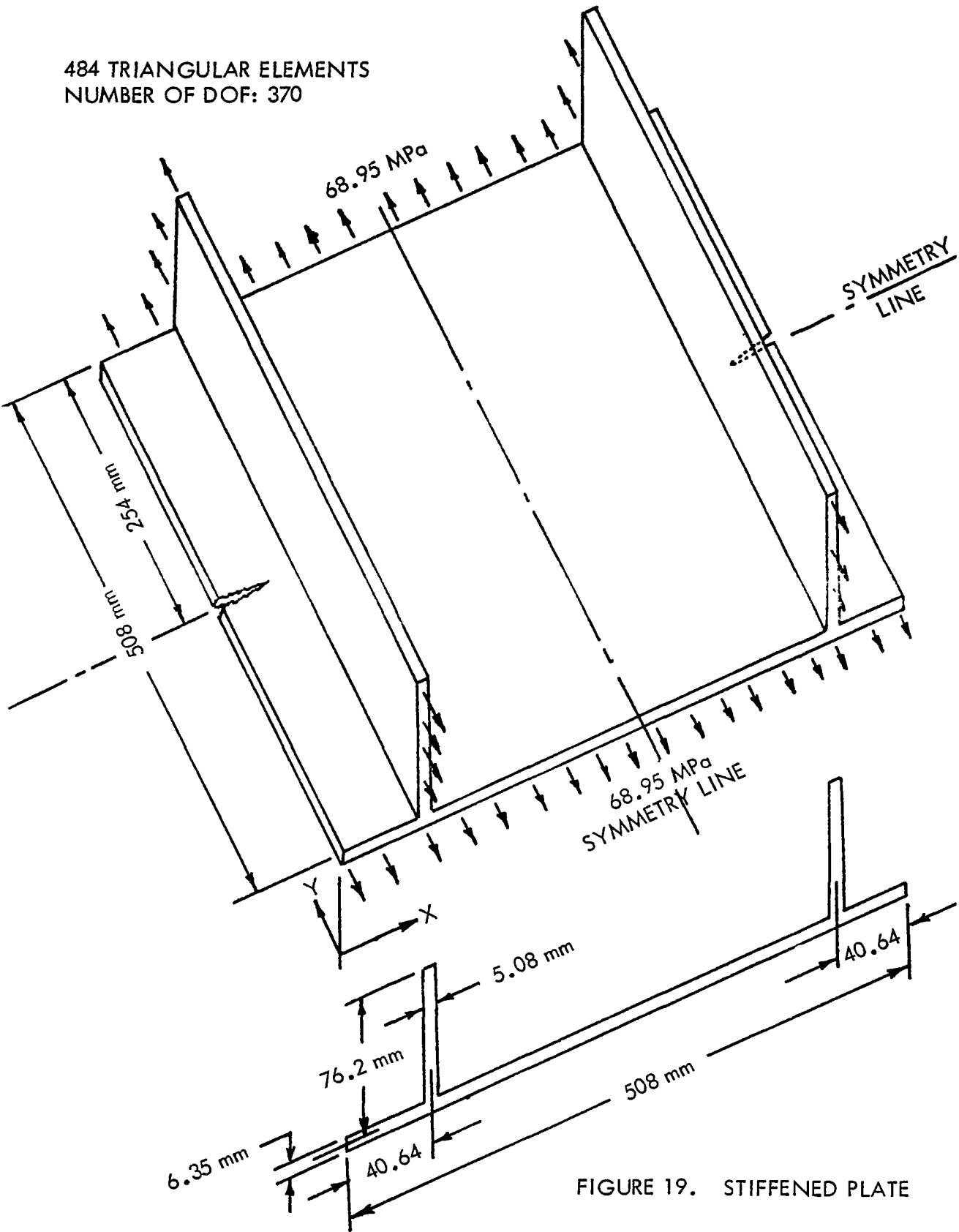
FIGURE 19.   STIFFENED PLATE
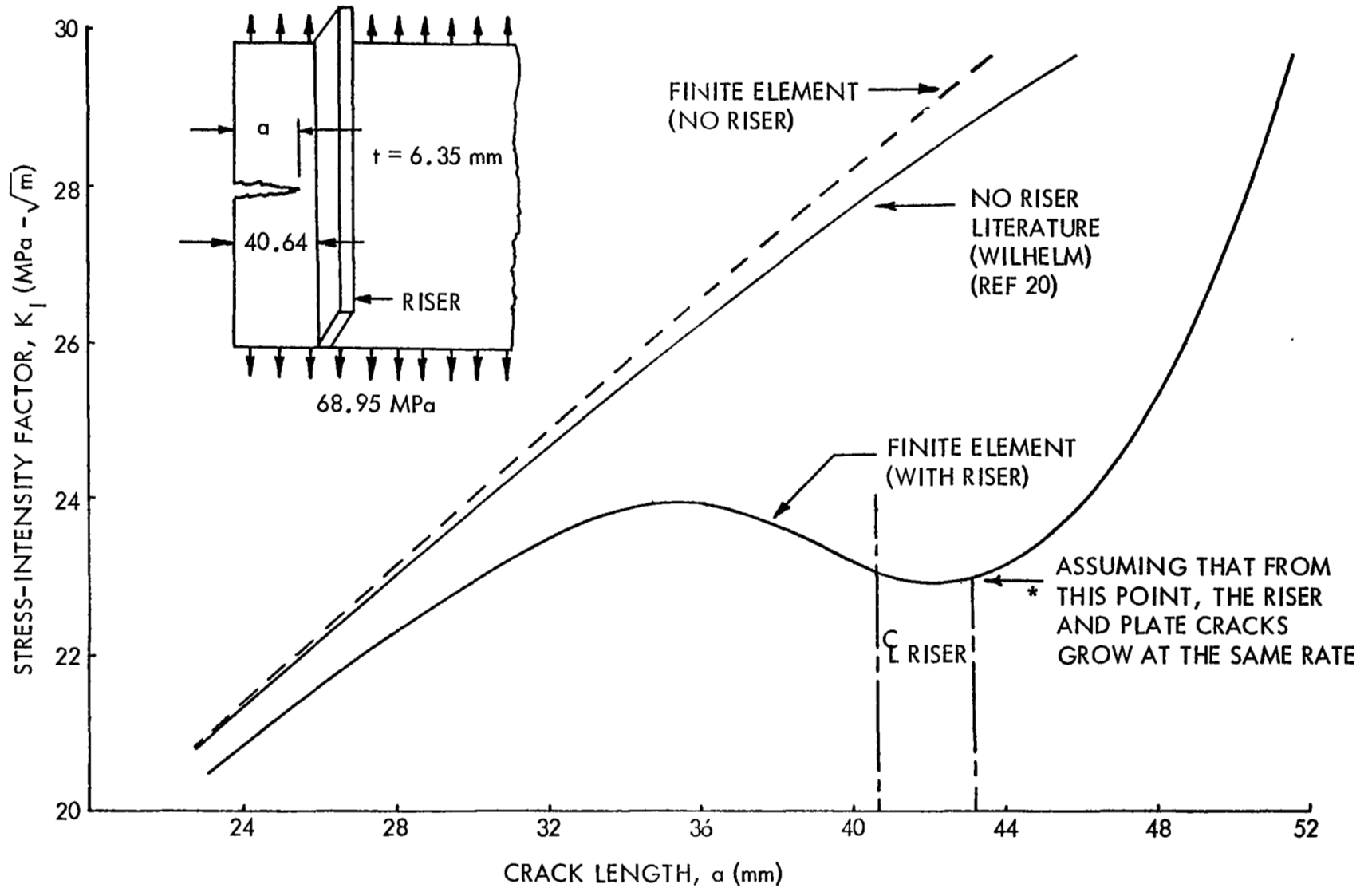
FIGURE 20.   EFFECT OF RISER ON STRESS INTENSITY IN PLATE
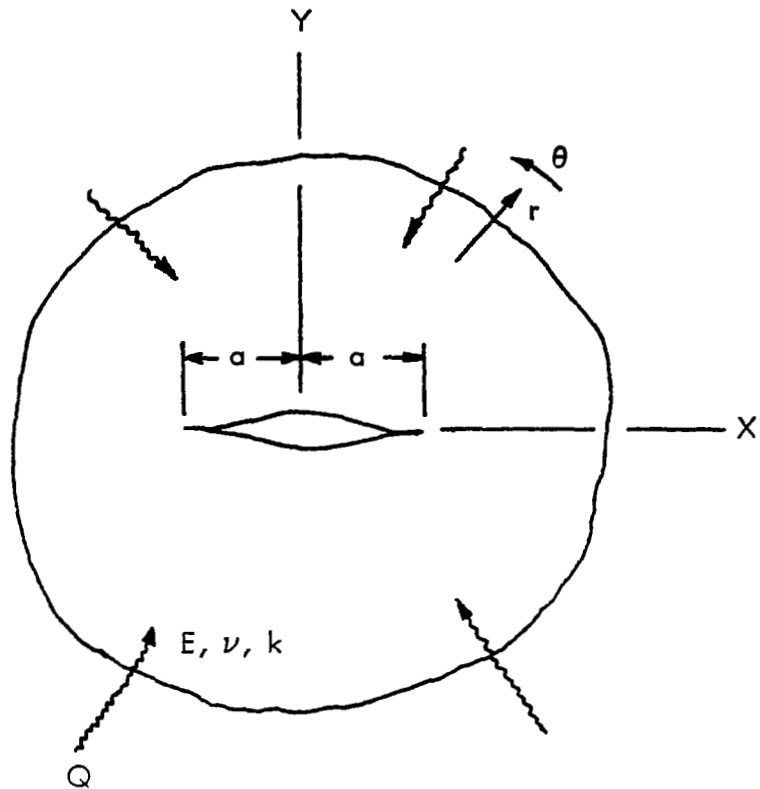
FIGURE 21. GEOMETRY OF THE THERMAL STRESS PROBLEM
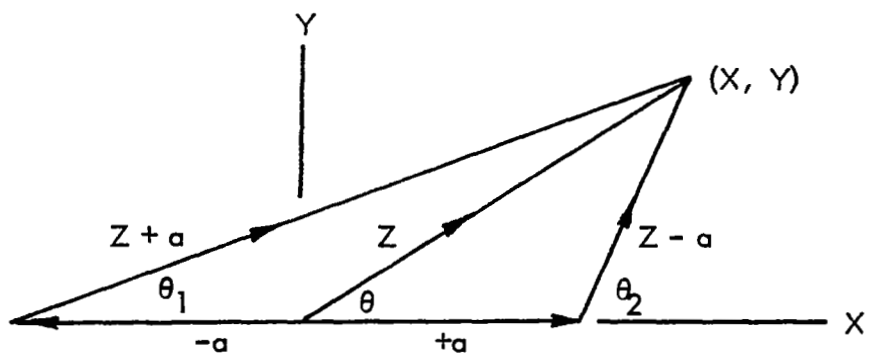
FIGURE 22. VECTOR REPRESENTATION FOR THERMAL PROBLEM
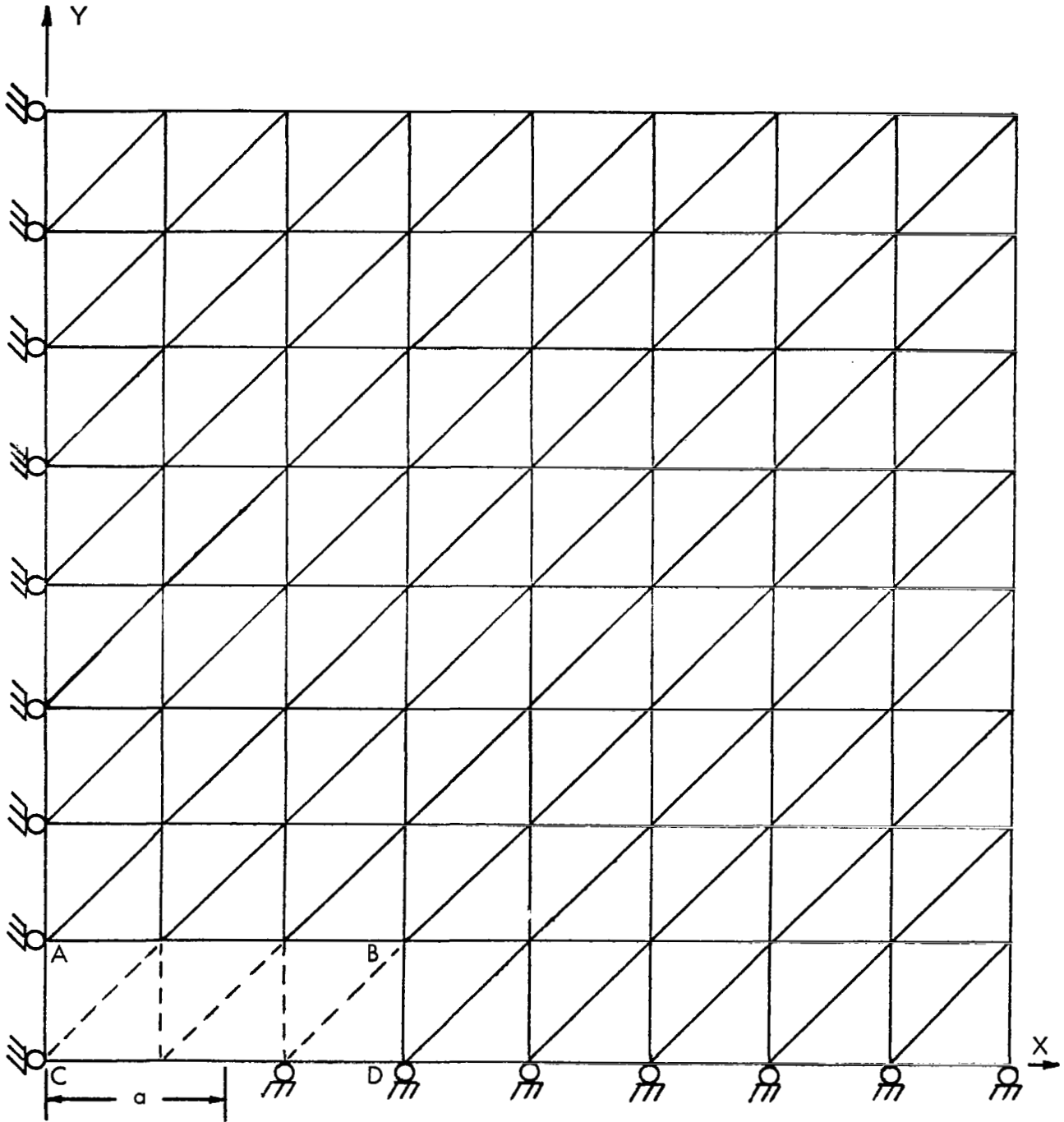
FIGURE 23.   FINITE-ELEMENT REPRESENTATION OF THERMAL STRESS PROBLEM
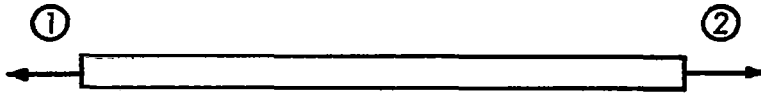
FIGURE A-1.   AXIAL ELEMENT
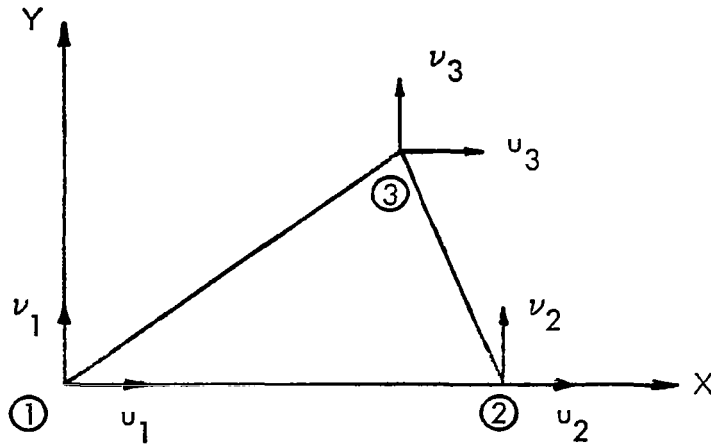
FIGURE A-2.   TRIANGULAR ELEMENT MEMBRANE
DISPLACEMENTS
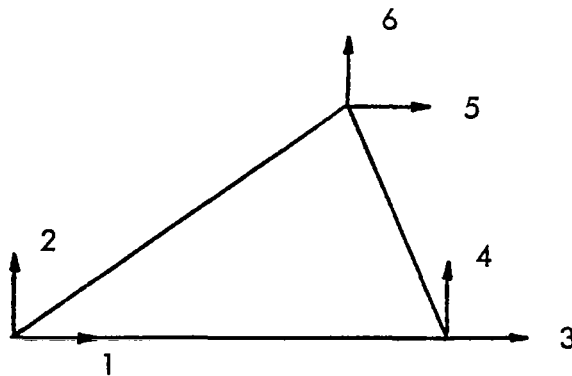
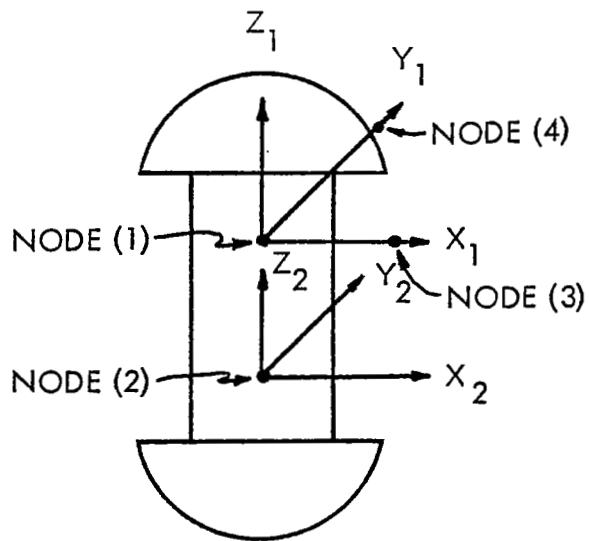FIGURE A-3.   CONVENTION FOR DEGREES OF
FREEDOM
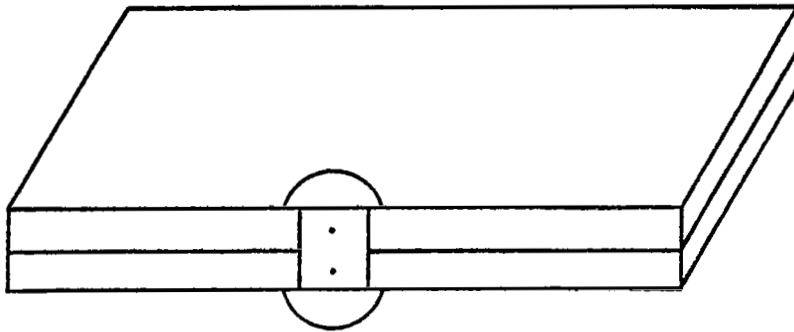
FIGURE A-4.   SHEAR PIN

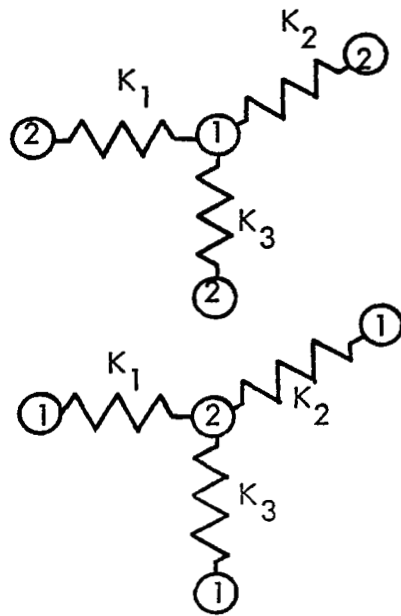FIGURE A-5.   DIRECTION VECTORS FOR FASTENER ELEMENT
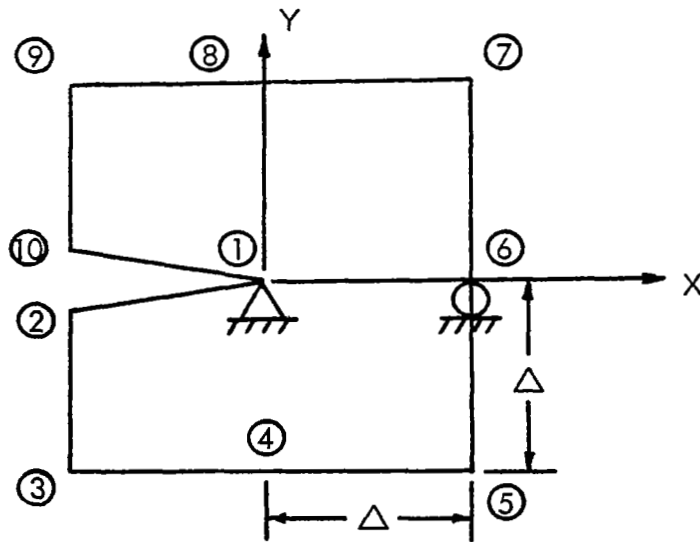
FIGURE A-6.   SPRING SYSTEM TO SIMULATE SHEAR PIN

FIGURE A-7.   LOCAL COORDINATE SYSTEM FOR
TEN-NODE CRACKED ELEMENT